NASA-CR-200057

Texas A&M University
Mechanical Engineering Department

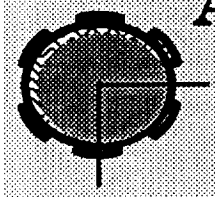

Angled Injection- Hybrid Fluid Film Bearings for Cryogenic Applications

Annual Research Progress Report to
NASA Lewis Research Center
NASA Grant NAG3-1434
Contract Monitor: Mr. James Walker

Luis San Andres
Associate Professor

December 1995

Period of performance: January 1 to December 31, 1995

Thermohydrodynamic Analysis of Cryogenic Liquid Turbulent Flow Fluid Film Bearings
(Phase III)

Texas A&M University
Mechanical Engineering Department

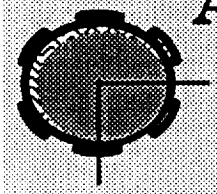

Angled Injection- Hybrid Fluid Film Bearings for Cryogenic Applications

Annual Research Progress Report to
NASA Lewis Research Center
NASA Grant NAG3-1434
Contract Monitor: Mr. James Walker

Luis San Andres
Associate Professor

December 1995

Period of performance: January 1 to December 31, 1995

Thermohydrodynamic Analysis of Cryogenic Liquid Turbulent Flow Fluid Film Bearings
(Phase III)

THERMOHYDRODYNAMIC ANALYSIS OF CRYOGENIC LIQUID TURBULENT FLOW FLUID FILM BEARINGS
PHASE III - December 1995

ANGLED INJECTION HYBRID FLUID FILM BEARINGS FOR CRYOGENIC APPLICATIONS

Luis San Andres
Associate Professor
Mechanical Engineering Department
Texas A&M University
College Station, TX 77843-3123

prepared for NASA Lewis Research Center
NASA Grant NAG3-1434, Phase III
Contract Monitor: Mr. James Walker

EXECUTIVE SUMMARY

A computational bulk-flow analysis for prediction of the force coefficients of hybrid fluid film bearings with angled orifice injection is presented. Past measurements on water-lubricated hybrid bearings with angled orifice injection have demostrated improved rotordynamic performance with virtual elimination of cross-coupled stiffness coefficients and nul or negative whirl frequency ratios. A simple analysis reveals that the fluid momentum exchange at the orifice discharge produces a pressure rise in the recess which retards the shear flow induced by journal rotation, and consequently, reduces cross-coupling forces. The predictions from the model correlate well with experimental measurements from a radial and 45° angled orifice injection, 5 recess water hybrid bearings (C=125 μm) operating at 10.2, 17.4 and 24.6 krpm and with nominal supply pressures equal 4, 5.5 and 7 MPa. An application example for a liquid oxygen 6 recess/pad hybrid journal bearing shows the advantages of tangential orifice injection on the rotordynamic force coefficients and stability indicator for forward whirl motions and without performance degradation on direct stiffness and damping coefficients. The computer program generated, ***hydrojet***, extends and complements prior codes developed on phases I and II of the project.

TABLE OF CONTENTS

THERMOHYDRODYNAMIC ANALYSIS OF CRYOGENIC LIQUID TURBULENT FLOW FLUID FILM BEARINGS PHASE III - December 1995

NOMENCLATURE

A_o	$C_d \pi d_o^2/4$. Effective orifice area [m^2].
b	recess circumferential length [m].
C	Radial clearance function [m].
C_p	Fluid specific heat [J/kg·°K].
$C_{XX}, C_{XY}, C_{YX}, C_{YY}$	Damping force coefficients [Ns/m].
C_d	Orifice discharge coefficient
D	2·R . Bearing diameter [m].
d_o	Orifice diameter [m]
$f_{J,B}$	$a_M \left[1 + \left(c_M \frac{r_{J,B}}{H} + \frac{b_M}{R_{J,B}} \right)^{e_M} \right]$; a_M=0.001375, b_M=500,000; c_M=10,000, e_M=1/3.00
	Turbulent flow friction factors at journal and bearing surfaces.
e_X, e_Y	Journal center eccentricity components [m]
F_X, F_Y	Bearing fluid film forces along {X,Y} axes [N].
h_X, h_Y	cos(θ), sin(θ)
H	$C + e_X(t) \cos(\theta) + e_Y(t) \sin(\theta)$. Film thickness [m].
H_r	Recess depth [m].
H_e	Effective film depth for rough surface bearing [m].
$K_{XX}, K_{XY}, K_{YX}, K_{YY}$	Bearing force stiffness coefficients [N/m]
L,l	Bearing axial length, recess axial length [m].
$M_{XX}, M_{XY}, M_{YX}, M_{YY}$	Bearing inertia force coefficients [kg].
P, P_r, P_s	Fluid pressure, recess pressure, supply pressure [N/m^2]
Q_o	$(\rho V_o A_o)$. Flow rate across orifice [kg/s].
Re	$(\rho \cdot \Omega \cdot C \cdot R/\mu)_*$. Nominal circumferential flow Reynolds number.
R_J, R_B	$(\rho/\mu)H\sqrt{[(U_x-\Omega\cdot R)^2+U_y^2]}$; $(\rho/\mu)H\sqrt{[U_x^2+U_y^2]}$

	Flow Reynolds numbers relative to journal and bearing surfaces.
r_J, r_B	Roughness depths at journal and bearing surfaces [m].
t	Time [s].
T, T_s	Temperature, supply temperature [°K].
U_x, U_y	Bulk-flow velocities in circ.(x) and axial (y) directions [m/s].
V_o	fluid velocity through recess orifice [m/s]
V_r	Recess volume including supply line [m^3].
W_X, W_Y	External loads applied on journal [N].
x, y	Coordinate system on plane of bearing [m].
X, Y	Inertial coordinate system [m].
α	Fluid swirl ratio at recess edges.
β_P	$(1/\rho)(\partial\rho/\partial P)$. Liquid compressibility coefficient [m^2/N].
β_T	$-(1/\rho)(\partial\rho/\partial T)$. Liquid volumetric expansion coefficient [1/°K].
δ	angle of injection on orifice of recess [rad].
ΔP_{rv}	Hydrodynamic pressure rise within recess [N/m^2]
ΔP_{rm}	Recess pressure drop due to momentum exchange [N/m^2].
θ	x/R. Circumferential or angular coordinate.
$\kappa_y = \kappa_x$	$\frac{1}{2}(\kappa_J + \kappa_B)$. Turbulence shear factors in (y,x) flow directions.
κ_J, κ_B	$f_J \cdot R_J$, $f_B \cdot R_B$. Turbulent shear parameters at journal and bearing surfaces.
ρ, μ	Fluid density [Kg/m^3], viscosity [Ns/m^2].
ξ_{xu}, ξ_{xd}	Empirical recess-edge entrance loss coefficients in circumferential (upstream,downstream) direction.
ξ_y	Empirical recess-edge entrance loss coefficients in axial direction.
Ω, ω	Rotational speed of journal, excitation or whirl frequency [1/s]

Subscripts refer to:

x,y	in direction of local circumferential and axial coordinates in plane of bearing.
o	orifice
r,e	bearing recesses and edges (entrance).
u,d	upstream and downstream of recess.
B,J	refer to bearing and journal surfaces.

LIST OF TABLES

LIST OF FIGURES

List of Figures (continued)

ANGLED-INJECTION HYBRID FLUID FILM BEARINGS FOR CRYOGENIC APPLICATIONS

Luis San Andres
Associate Professor
Mechanical Engineering Department
Texas A&M University
College Station, TX 77843

December 1995

ABSTRACT

A computational bulk-flow analysis for prediction of the performance and force coefficients of hybrid (combined hydrostatic - hydrodynamic) bearings with angled orifice injection is presented. Hybrid fluid film bearings bearings for cryogenic turbopumps offer reliabity with maximum operating life and optimum controllable rotordynamic characteristics at the lowest cost. However, fixed geometry hybrid bearings have limited hydrodynamic stability characteristics. Measurements on water hybrid bearings with angled orifice injection have demostrated improved rotordynamic performance with virtual elimination of cross-coupled stiffness coefficients and null or negative whirl frequency ratios. The analysis reveals that the fluid momentum exchange at the orifice discharge produces a pressure rise in the recess which retards the shear flow induced by journal rotation, and consequently, reduces cross-coupling forces. The predictions from the model are compared with experimental measurements for a 45° angled orifice injection, 5 recess water hybrid bearing operating between 10.2 krpm to 24.6 krpm and with supply pressures from 4 to 7 MPa. The correlations include load and flow rates versus journal eccentricity, and rotordynamic force coefficients at the journal centered position. An application example for a liquid oxygen hybrid bearing also demonstrates the advantages of an angled orifice injection design on the rotordynamic coefficients and stability indicator without performance degradation.

INTRODUCTION

The importance of hybrid (combination hydrostatic and hydrodynamic) journal bearings as reliable support elements in cryogenic turbomachinery has steadily grown over the past few years. Hybrid journal bearings (HJBs) enable smaller and lighter turbopumps through no bearing DN life limitation and no sub-critical rotor operation. HJBs have durability, low friction and wear, accuracy of positioning, and large direct stiffness and damping force coefficients. The growth of an "all-fluid-film-bearing" technology for advanced and less expensive (per launching cost) turbopumps has required the development of analytical models and design tools, the testing of components, and the implementation of the technology (Pelfrey, 1995).

Primary power cryogenic turbomachinery operates at high speeds and produces large fluid pressure rises (max. 30 MPa). These typical operating conditions determine the flow in the supporting fluid film bearing to be fully turbulent with dominance of fluid inertia and thermal transport effects. San Andres (1990-1995) provides bulk-flow analyses and computational programs for the calculation of bearing performance and rotordynamic force coefficients. These analyses have grown steadily in complexity and include unique features to model with exactness the flow in cryogenic liquid bearings.

Measurements of bearing rotordynamic force coefficients and load performance are routinely performed at a high-speed Hydrostatic Bearing Test Facility (HBTF) (Childs and Hale, 1994). Tests have been conducted with water for more than 30 hybrid journal bearings and damper seals with rotational speeds ranging from 10 to 25 krpm and pressure differentials from 4 to 7 MPa. The facility accomodates state of the art instrumentation with remotely controlled testing, and includes an efficient real-time parameter identification method based on frequency domain

techniques. Kurtin et al. (1993), Franchek et al. (1994, 95), Mosher and Childs (1995), and Yang et al. (1995) report extensive experimental data for the static performance characteristics of a 5 recess HJB for the operating conditions noted and three different bearing clearances (76 to 127 μm). These studies demonstrate that predictions from the computational bulk-flow models correlate favorably with the experimental results. Accurate predictions depend greatly on the knowledge of the bearing operating clearances, and most importantly, on the orifice discharge coefficients. The references cited along with San Andres (1995a) also discuss the sensitivity of the computed predictions to variations in the input empirical parameters.

Despite the many advantageous features offered by HJBs, hydrodynamic and "pneumatic-hammer" stability limits and two-phase flow operation are of primary concern for high speed operation with large pressure differentials. Fluid vaporization is possible since the cryogenic liquid enters the bearing (or seal) at conditions close to its saturation temperature. The large mechanical energy dissipated by the fluid motion is convected by the fluid and changes greatly its thermophysical state while the pressure drops to the exit plane of the bearing. "Pneumatic hammer" effects are avoided by appropriate selection of the flow restrictor, by designing bearing recesses with small volumes, and by restricting bearing operation to flow conditions where the pressure differential is a small fraction of the liquid bulk modulus (Redecliff and Vohr, 1969). This last condition is difficult to achieve in bearings employing liquid hydrogen due to its large compressibility.

The stability of a simple rotor-bearing system is defined by its threshold speed and the whirl frequency ratio (WFR). The instability of "hydrodynamic" type is solely due to the effect of journal rotational speed on the bearing flow

field. The threshold speed corresponds to the rotor speed at which a bearing is deprived from its effective damping and any small perturbation from an equilibrium position will determine unbounded rotor motions. The WFR denotes the ratio between the onset whirl frequency (typically the system first critical speed) and the threshold speed of instability. This stability indicator is independent of the flexibility of the rotating shaft. Plain journal bearings show a WFR equal to 0.50 for small to moderate operating eccentricities (light loads), and thus demonstrate instability at a rotational speed equal to twice the system first critical speed. Measurements in hybrid bearings verify closely the theoretical WFR prediction. In some circumstances the WFR even increases above 0.50, in particular for low rotational speeds and large supply pressures (Franchek, 1992, Franchek et al. 1995).

The WFR=0.50 condition limits severely the application of HJBs to high speed, light weight turbomachinery, and thus, the research has concentrated on conceiving hybrid bearings with improved stability and without loss in centering stiffness and damping ability. Some of the technological advances have been the natural outcome of analysis and engineering design, while others follow empirical evidence and past experience when a mathematical model is yet to be crafted. Other recommended fixes to improve the hydrodynamic stability of hybrid bearings by reducing or eliminating the WFR are the following:

- o Use of machine roughened bearing surfaces to decrease the cross-coupled stiffness coefficients. Test results show a rough knurled-pattern HJB to have a WFR as low as 0.30 but with a reduced load capacity and direct stiffness when compared to a smooth surface HJB (Franchek, 1992).
- o Use of circumferentially asymmetric pad bearings and recesses to produce enough anisotropy on the rotordynamic force coefficients. Measurements and

analysis for an engineered two pad HJB validated the concept (San Andres, 1995b). However, this bearing configuration is highly sensitive to the direction of applied static loads.

- o Use of flexure-pivot, tilting pad HJBs or compliant surface (foil) journal bearings due to their inherent stability. San Andres (1995c, 1994) discusses at length these concepts and evaluates their potential for cryogenic uses. Flexure-pivot HJBs constitute a novel altenative and full-scale testing is planned for the first semester of 1996. Foil bearings have also demonstrated their performance in cryogenic turbomachinery (Genge et al., 1993). The current foil bearing technology allows only for specific loads applicable to secondary power cryogenic turbopumps. The interested reader should recall the cited references for further details.
- o Use of hybrid bearings with angled liquid injection opposing journal rotation to reduce the development of the circumferential flow velocity and with virtual elimination of cross-coupled stiffness coefficients. This concept has lacked firm theoretical modeling though it has proved successful in some applications (Tondl, 1967, Brown and Hart, 1986). Experimental measurements for a 5 recess HJB demonstrate that angled injection aids in reducing the whirl frequency ratio without decreasing the bearing centering stiffness and load capacity (Franchek, 1992, Franchek and Childs, 1995).

This report presents the thermohydrodynamic analysis of real properties, hybrid bearings with angled orifice injection. The objective is to advance a computational model able to predict reliably the performance of angled injection HJBs in lieu of their favorable (measured) rotordynamic performance. The motion of a fluid through the thin film lands is governed by mass, momentum and energy transport equations for the bulk-flow velocities, pressure and temperature,

along with thermophysical state equations for evaluation of the cryogen material properties. The turbulent bulk-flow is modeled with simple friction coefficients and include effective film depths to accomodate for macroscopic surface roughness. A simple analysis for the angled injection - orifice flow reveals that the fluid momentum exchange produces a pressure rise in the recess which retards the shear flow induced by journal rotation. Zeroth-order equations describe the fluid flow field for a journal static equilibrium position, while first-order linear equations govern the fluid flow for small amplitude journal center translational motions. Solution to the zeroth-order flow equations provides the bearing flow rate, shear torque and load capacity. Solutions to the first-order equations determine the linearized rotordynamic stiffness, damping and inertia force coefficients as functions of a whirl frequency. The numerical predictions from the model are correlated extensively with the experimental data of Franchek (1992).

ANALYSIS

Figure 1 shows the geometry of a hybrid (combination hydrostatic/hydrodynamic) journal bearing and the relevant nomenclature. A liquid at high pressure (P_s) and inlet temperature (T_s) is supplied (radially or angled) through orifice restrictors and impinges into the bearing recesses with a mean pressure (P_r). The pressure field within the recesses is determined from flow continuity with the film lands, momentum exchange at the orifice plane and a viscous rise due to journal rotation. At the recess edges, an inertial pressure drop also occurs due to the sudden transition from the recess of depth (H_r) into the film land regions of small thickness (H). Past the recesses, the liquid then flows through the film lands and the pressure drops to the discharge value (P_a).

Equations of flow on the bearing film lands

On the thin film lands flow turbulence, fluid inertia and compressibility effects are important. The model then assumes a fully developed turbulent bulk-flow of a fluid whose material properties depend on its local thermophysical state of pressure and temperature. The equations of mass, axial and circumferential momentum, and adiabatic-flow energy transport for the bulk-flow velocities, pressure and temperature in the bearing film lands are given as (Yang et al., 1995, Kleynhans and Childs, 1995):

$$\frac{\partial}{\partial t}(\rho H_e) + \frac{\partial}{\partial y}(\rho H U_y) + \frac{\partial}{\partial x}(\rho H U_x) = 0 \qquad (1)$$

$$-H\frac{\partial P}{\partial y} = \frac{\mu}{H}\left\{K_y U_y\right\} + \frac{\partial(\rho H_e U_y)}{\partial t} + \left\{\frac{\partial(\rho H U_y U_y)}{\partial y} + \frac{\partial(\rho H U_y U_x)}{\partial x}\right\} \qquad (2)$$

$$-H\frac{\partial P}{\partial x} = \frac{\mu}{H}\left\{K_x U_x - K_J\frac{\Omega R}{2}\right\} + \frac{\partial(\rho H_e U_x)}{\partial t} + \left\{\frac{\partial(\rho H U_y U_x)}{\partial y} + \frac{\partial(\rho H U_x U_x)}{\partial x}\right\} \qquad (3)$$

$$C_p\left\{\frac{\partial}{\partial t}\left(\rho H_e T\right) + \frac{\partial}{\partial x_\alpha}\left(\rho H U_\alpha T\right)\right\} = \beta_T H T\left\{\frac{\partial P}{\partial t} + U_\alpha\frac{\partial P}{\partial x_\alpha}\right\} + \Omega\cdot R\,\frac{H}{2}\frac{\partial P}{\partial x}$$

$$+ \frac{\mu}{H}\left\{K_x\left(U_x^2+U_y^2+\frac{1}{2}\Omega\cdot R\cdot U_x\right) + K_J\Omega R\left(\frac{1}{4}\Omega R - U_x\right)\right\} \qquad (4)$$

$\alpha = x, y$

Please refer to the Nomenclature for a description of all variables. $K_y = K_x = (k_J + k_B)/2$ are the wall shear stress parameters determined as local functions of turbulent friction factors which depend on the bearing and journal surface conditions and the flow Reynolds numbers relative to the rotating (R_J)

and stationary (R_B) surfaces, i.e $\kappa_J=f_J\cdot R_J$, $\kappa_B=f_B\cdot R_B$ (Hirs, 1973). The cryogenic liquid properties are extracted from the Benedict-Web-Rubin equation of state as given in the standard data base of McCarty (1986).

The fluid pressure at the sides of the bearing ($y=\pm L/2$) equals the discharge or ambient value (P_a). At the interface with the bearing recesses, continuity of flow and pressure must be attained as detailed below.

Angled Injection - Recess Flow and Pressure equations

Figure 2a depicts a hydrostatic bearing recess (or pocket) with axial length **(l)** and circumferential extent **(b)**. The figure shows the direction of the journal surface speed **($\Omega\cdot R$)**, and relative to this velocity the recess is divided into upstream **(u)** and downstream **(d)** regions. The fluid supply orifice port with injection angle **(δ)** is located at a distance b_u from the upstream recess edge. The orifice has an effective area A_o normal to the feed speed V_o. Radial fluid supply is indicated by $\delta=0$ while a tangential feed opposite to journal rotation is given by $\delta=\pi/2$ (90°).

Conventional analysis of hydrostatic bearings do not calculate the flow field within the recess since these are typically deep and enclose large nearly stagnant fluid volumes. Analysis then accounts only for flow continuity with the film lands and determines a (uniform) recess pressure using a simple orifice equation based on Bernoulli's principle. The complexity of the flow field in hydrostatic pockets has been discussed by Hill et al. (1995) and Braun et al. (1993, 1995) with the aid of two-dimensional computational fluid mechanics analyses. Numerical results reveal the generation of hydrodynamic pressures within the pocket and followed by sharp inertial pressure drops at the recess edges. This field of study is of utmost importance for the development of a mature technology on hybrid bearings for cryogenic applications.

The analysis of angled injection - hydrostatic pockets follows here a simplified approach which intends to be of practical use without resorting to computationally intensive three dimensional flow calculations. The flow model is evidently crude yet it grasps the fundamental mechanisms of pressure generation within the bearing pockets. The favorable correlation with hybrid bearing experimental performance characteritics given later justifies the method used.

A mass conservation equation at each bearing recess of area $(l \cdot b)$ and depth H_r is defined by the global balance between the mass flow through the orifice restrictor (Q_{ro}), the mass flow into the film lands and the time rate of change of liquid mass within the recess and supply line volume (V_r), i.e.

$$Q_{ro} = \rho_r A_o V_o = \iint_{\Gamma_r} \left[\rho H \vec{U}.\vec{n} \right] d\Gamma_r + \frac{\partial}{\partial t}(\rho_r V_r) \qquad (5)$$

for r=1,2..., Nrecess

where $A_o = C_d \pi d_o^2/4$ is the effective orifice area with C_d as an empirical discharge coefficient. Γ_r denotes the closure of the recess with the film lands and has a normal n along the boundary line. At the orifice discharge plane, the mean recess pressure is denoted by P_r (see Figure 2b) and given from Bernoulli's equation as:

$$(P_s - P_r) = (1/2)\ \rho_r\ V_o^2 \qquad (6)$$

Computational fluid mechanics analysis reveals that the axial pressure within the recess is (to a first approximation) practically uniform. Hence, modelling of the flow in the pocket as a one-dimensional bulk-flow bearing determines that the pressure difference (downstream - upstream) on a recesses is given by two

contributions:

a) a viscous pressure rise (ΔP_{rv}) due to shear flow (San Andres, 1992):

$$\Delta P_{rv} = \left[P_d - P_u \right]_v = \mu_r K_{xr} \frac{b}{H_r^2} \left(\frac{\Omega \cdot R}{2} - U_{rx} \right) \qquad (7)$$

b) a pressure drop (ΔP_{rm}) at the orifice injection plane and due to the exchange of fluid momentum, and simply stated as:

$$\Delta P_{rm} = \left[P_d - P_u \right]_m = - \frac{Q_o \, V_o \, \sin(\delta)}{H_r \cdot l} = - \frac{2 \, A_o}{H_r \cdot l} \cdot (P_s - P_r) \, \sin(\delta) \qquad (8)$$

where the orifice equation (6) has been used on the right hand side of eqn (8). Note that for radial injection (δ=0) there is no momentum pressure drop at the supply port. The viscous pressure rise depends greatly on the journal speed and the mean recess circumferential flow speed. On the other hand, the momentum exchange pressure drop is the largest for large pressure differentials (P_s-P_a) and tangential injection (δ=90°). For simplicity the pressure field within the hydrostatic pocket is then taken as linear and combines the two pressure differences as shown pictorially in Figure 2b. Note that this simplification avoids the calculation of the complex flow field on the entire bearing recess.

Finally, the entrance pressures (P_e) to the film lands in the circumferential (upstream and downstream) and axial directions are given by (San Andres, 1992):

$$P_e \Big|_{u,d} = \left[P_r - \frac{\rho}{2} (1+\xi_x) \left\{ 1 - U_x^2 \right\} \right]_{u,d} \qquad (9.a)$$

$$P_e = P_r - \frac{\rho}{2} (1+\xi_y) \left\{ 1 - U_y^2 \right\} \qquad (9.b)$$

The analysis generalizes equations (9) for uneven empirical entrance loss factors ξ in the upstream(u) and downstream(d) sections of the recess. Equations (9) are used only when fluid flows from the recess towards the film lands.

Perturbation Analysis

Consider the motion of the journal as the superposition of small amplitude periodic motions of frequency **(ω)** around a static equilibrium position. That is, the journal center displacements are given as

$$e_X(t) = e_{Xo} + \Delta e_X\, e^{i\omega t}, \quad e_Y(t) = e_{Yo} + \Delta e_Y\, e^{i\omega t}; \quad i=\sqrt{-1} \qquad (10)$$

The magnitudes of the dynamic perturbations in journal displacements are small, i.e., $|\{\Delta e_X, \Delta e_Y\}| \lll C$. The film thickness **(H)** can then be regarded as the superposition of a steady-state **(H_o)** and dynamic components given by the real part of the following expression:

$$H = H_o + \{\, \Delta e_X\, h_X + \Delta e_Y\, h_Y \,\}\, e^{i\omega t} \qquad (11)$$

where $H_o = C(y) + e_{Xo}\, h_X + e_{Yo}\, h_Y$; and $h_X = \cos(\theta)$, $h_Y = \sin(\theta)$

The flow field variables (U_x, U_y, P, T), as well as the fluid properties (ρ, μ) and the shear parameters (K_x, K_y) are also formulated as the superposition of zeroth-order and first-order complex fields describing an equilibrium for steady-state flow, and the perturbed condition for small amplitude dynamic journal motions, respectively. In general, these fields are expressed as:

$$\Psi = \Psi_o + \left\{\Delta e_X \Psi_X + \Delta e_Y \Psi_Y\right\} e^{i\omega t} \qquad (12)$$

Substitution of equations (11) and (12) into the flow equations (1-9) renders

zeroth- and first-order equations for determination of the steady-state and perturbed flow-fields. These equations are not reproduced here for brevity but can be found in their full extent in the reference of San Andres (1993). The bearing static and dynamic force characteristcis are evaluated once a solution to the flow equations is obtained. Fluid film forces (F_X,F_Y) and force coefficients (stiffness $K_{\alpha\beta}$, damping $C_{\alpha\beta}$ and inertia $M_{\alpha\beta}$) are calculated by integration of the pressure fields over the journal surface. The appropriate formulae are:

$$F_\alpha = \int_0^L \int_0^{2\pi} P_o \, h_\alpha \, R \cdot d\theta \cdot dy; \qquad \alpha = X,Y \tag{13}$$

$$K_{\alpha\beta} - \omega^2 M_{\alpha\beta} + i\omega C_{\alpha\beta} = \int_0^L \int_0^{2\pi} P_\beta \, h_\alpha \, R \cdot d\theta \cdot dy; \qquad \alpha,\beta = X,Y \tag{14}$$

Numerical method of solution

The control-volume method of Launder and Leschziner (1978) is used to solve the differential equations of motion. Staggered grids containing control volumes for the primitive flow variables (circumferential and axial velocity, pressure and temperature) cover the flow domain. Algebraic difference equations are derived on each control volume for the conservation of mass, axial and circumferential momentum, and balance of energy. A pressure correction equation is derived using the SIMPLEC procedure of Van Doormaal and Raithby (1984). A Newton-Raphson scheme is also used for satisfaction of the recess mass flow constraint. Full descriptions on the accuracy and parameter sensitivity of the method as applied to hybrid bearings and annular pressure seals are given in

past publications (San Andres, 1990-1995). The interested reader should consult the cited references for a detailed exposition of the numerical method used.

The computer program generated in fortran-77 is named **hydrojet** and it is based on the original code **hydrosealt** developed earlier (San Andres, 1993). **hydrojet** is fully compatible with its predecessors including **hydroflext** and keeps the same basic structure and user friendly interface. **hydrojet** is available from Texas A&M University Technology Licensing Office.

COMPARISONS TO TEST RESULTS FROM A WATER 5-RECESS HYBRID BEARING

Franchek (1992) presents an experimental study of five hybrid bearings with distinctive geometrical configurations. These are namely, smooth bearings with radial injection and rectangular (baseline), triangular and circular recesses, a knurled rough-surface bearing with rectangular recesses, and a smooth surface bearing with rectangular recesses and a 45° angled orifice injection. The tests consisted of the measurement of load vs. journal eccentricity, torque and flow rate, and the identification of rotordynamic force coefficients (stiffness, damping and inertia) using a random frequency shaker excitation system. Childs and Hale (1994) provide a full description of the test apparatus and the experimental procedure. The **nominal** test conditions include:

(a) 3 rotational speeds: 10.0, 17.4 and 24.6 krpm
(b) 3 supply pressures: 4.0, 4.5 and 7.0 MPa (600, 800 and 1000 psig)
(c) 6 journal eccentricity ratios (e/c): 0.0 to 0.5
at a supply temperature of 55°C (130°F).

Franchek and Childs (1994) and Franchek et al. (1995) briefly report the measurements in the archival literature with comparisons to predictions from the present analysis for the baseline bearing (radial injection). Table 1 describes

the geometry of the test hybrid bearings with radial and angled (45°) injection. At the journal centered position the measured data for flow rate, supply and average recess pressures and operating clearance is also given. From these values, empirical orifice loss coefficients (C_d) are estimated for each test condition and used in all computations including journal off-centered operations. The values of circumferential (Re_c) and axial flow Reynolds (Re_a) numbers demonstrate the character of the flow within the test bearings. The experimental measurements along with predictions from the current numerical model follow. Angled and radial injection results are presented at the top and bottom of the figures, respectively, and with measurements depicted in broken lines and predicted values in continuous lines.

Static Performance Characteristics of test bearings

Figure 3 depicts the journal eccentricity versus applied load (W_X) for both bearings at a nominal supply pressure of 7.0 MPa and three rotational speeds. The journal eccentricity increases almost linearly with the applied load which is typical of externally pressurized bearings. This also demonstrates that the stiffness coefficients for the bearings will not vary (greatly) with the journal center position. An increment in the operating speed produces a rise in the load capacity (smaller eccentricities) with both bearings having similar load capacities. The model calculated results agree best with the angled injection tests. Figure 4 shows the predicted journal center locii for both bearings. Test results are not shown since these are not included on Franchek's work (1992). Note that for the radial bearing, the journal locus presents a greater attitude angle as the journal speed increases. On the other hand, the angled injection results show a negative attitude angle at the lowest speed (10.2 krpm), an almost null angle at the medium speed (17.4 krpm), and increasing as the speed

reaches its highest value (24.6 krpm). The predictions reveal the fundamental differences between the two bearings. Thus engineering design could lead to a hybrid bearing free of cross-coupling effects with the appropriate combination of injection angle, supply pressure and operating speed.

Figures 5 and 6 show the predicted (dimensionless) film pressures at the midplane of the bearing for the centered condition (no load) and at a load (W_X) equal to 10 kN and directed towards the middle of a recess. Note that for concentric operation the angled injection bearing shows a recess pressure field significantly different from that for the radial injection HJB. As modeled, the exchange of momentum in the recess produces a pressure rise in the direction opposite to journal rotation which retards the development of the cicrcumfer - ential flow velocity. The effect is most pronounced at the lowest rotational speed (10.2 krpm). The recess pressures increase with the rotational speed denoting a rise in the flow resistance within the bearing film lands.

Figure 7 depicts the recess pressure ratios $\{(P_r-P_a)/(P_s-P_a)\}$ at the journal concentric position for the three nominal supply pressures and speeds. Recess pressure ratios rise with the journal speed and decrease with supply pressures since land flow resistance and turbulence are greater. The correlations with the model predictions are regarded as satisfactory except at the largest speed and lowest supply pressure. Note that the comparisons have been made with averaged test recesses pressures. Actual measured recess pressures within the bearing vary as much as 13% from the calculated test average.

Figure 8 shows the predicted flow rates to agree closely with the measurements for both bearings at the centered journal position. The flow rate increases with supply pressure and decreases significantly with speed for the radial (baseline) bearing. On the other hand, the angled (45°) injection bearing

shows a less pronounced drop as speed rises while the model predictions show the opposite behavior. The rationale for the discrepancy is attributed to the larger predicted recess pressures with the model.

Figure 9 shows the comparisons between measured and calculated drag shear torques at the journal centered position. It is noted that the measurements refer to the torque on the bearing surface which may differ from that on the journal. Furthermore, the measurements at the lowest speed (10.2 krpm) are unusually low considering the size and operating conditions of the bearing. It appears as if the test torque is shifted by a constant amount for both bearings. Nevertheless, the measurements (and predictions) show that the drag torque is practically independent of the external supply pressure (P_s) and increases in a way not (linearly) proportional to journal speed due to the turbulent flow character of the test bearing. Most importantly, the angled injection bearing presents a smaller torque than the radial injection bearing and thus, it indicates that shear power losses are also smaller for this hybrid bearing configuration.

Dynamic Performance Characteristics at journal centered position

The test results and numerical predictions demonstrate that the rotordynamic force coefficients are practically insensitive to the applied load for journal eccentricities to 50% of the bearing clearance. Hence, in the following, only force coefficients at the concentric position are presented and thouroughly discussed.

The whirl frequency ratio (**WFR**), a stability parameter of paramount importance for the application of hybrid bearings to high speed applications, is depicted in Figure 10. The radial bearing presents a WFR close to 0.50 for most operating conditions and indicates its relatively poor stability, in particular

at low speeds and high supply pressures. On the other hand, the angled (45°) injection bearing shows a (large) negative WFR at the lowest speed and raising to the 0.5 limit as the rotational speed increases. The numerical predictions agree well with the measurements at the middle and high speeds, i.e. 17.4 and 24.6 krpm.

Figure 11 depicts the cross-coupled stiffness coefficients (K_{XY}=-K_{YX}) as the journal speed increases for three nominal supply pressures. In the radial injection bearing, the cross-coupled stiffness are always positive and increase with the journal speed. On the other hand, the angled injection bearing presents negative cross-coupled coefficient at the lowest speed. From a rotordynamics point of view this is a desired occurrence since then these dynamic coefficients provide forces damping the development of forward whirl motions. The identified experimental results show some variations between K_{XY} and $-K_{YX}$ which are most pronounced for the radial injection bearing. The numerical predictions show the same trends as the measurements but do not agree well with the measurements. The discrepancies (even with the radial injection bearing) could be attributed to the limitations of the bulk-flow model on handling reverse flow conditions.

Figure 12 presents the direct stiffness coefficients (K_{XX}=K_{YY}) versus the journal speed and nominal supply pressures. The angled (45°) injection bearing has larger direct stiffnesses at the lowest speed and largest supply pressure. However, both bearings have similar stiffness values at the largest speed tested. The experimental results show significant discrepancies between K_{XX} and K_{YY} and attributed to minute differences in the diameters of the feeding orifices. The numerical predictions agree very well with the measurements except at the lowest speed and highest pressure where the tests show an unexpected behavior.

The direct damping coefficients (C_{XX}=C_{YY}) are shown in Figure 13. The model predictions show similar damping values for both bearings and these coefficients raise with the journal speed. On the other hand, the test results show damping to decrease with speed for the radial bearing and the opposite effect for the angled injection bearing. Note also that the dicrepancies between test C_{XX} and C_{YY} are significant for the radial injection bearing. In general, the model calculations agree best with the angled injection HJB test results, although direct damping is underpredicted by as much as 25% at 24.6 krpm.

Figure 14 shows the predicted cross-coupled damping coefficients (C_{XY}=-C_{YX}) to increase with journal speed and with little influence of the external supply pressure. On the other hand, the test results show a different behavior with cross-damping coefficients being the largest at the middle test speed (17.4 krpm). No conclusive remark can be made in regard to the correlation of prediction and identified test coefficients.

Figures 15 and 16 show the direct inertia (M_{XX}=M_{YY}) and cross-coupled inertia (M_{YX}=-M_{XY}) force coefficients, respectively. The numerical predictions demonstrate these added mass coefficients to be practically independent of external supply pressure and with a slow variation as the journal speed increases. The experimentally identified inertia coefficients are of the same order of magnitude as the predictions but present unique features yet to be fully understood. The test direct inertia coefficients do not follow a clear trend and show the largest values at the middle test speed (17.4 krpm). For the radial (45°) injection bearing, negative direct inertia coeficients at 10.4 krpm actually may indicate a dynamic stiffnening of the hybrid bearing. The predictions evidently do not agree well with the test results. However, Franchek and Childs (1994) indicate the test inertia coefficients have average uncertainties

of 53%, thus explaining the erratic behavior of these parameters.

HYBRID BEARING EXAMPLE FOR A LIQUID OXYGEN APPLICATION

Table 2 contains design data for a liquid oxygen (T_s=90°K), 6 pad/recess hybrid bearing operating at 25 krpm and with a pressure drop (P_s-P_a) equal to 17.9 MPa. The application corresponds to an Advanced Launching System (ALS) turbopump configuration (San Andres, 1995c). The analysis for journal centered operation investigates the effects of the angle of fluid injection on the performance characteristics of the bearing. An injection angle equal to 0° indicates radial fluid supply while an angle equal to 90° denotes tangential injection against journal rotation.

Figure 17 presents the bearing whirl frequency ratio (WFR), flow rate, mean recess pressure ratio $(P_r-P_s)/(P_s-P_a)$ and maximum pressure (p_{rmax}) within the recess versus increasing values of the injection angle angle (δ). The flow rate and recess pressure ratio remain practically constant for all injection angles while the maximum recess pressure retarding the development of journal rotation steadily increases and becomes a maximum for tangential injection. The most important result concerns the whirl frequency ratio which decreases from a value close to 0.60 for radial injection to approximately -0.53 for tangential injection.

Figure 18 depicts the drag shear torque on the journal surface, and the maximum exit and mean exit fluid ($T_{|y=\pm L/2}-T_s$) temperature differences. The shear torque decreases dramatically due to the effect of the fluid injection opposing the journal rotation. The temperatures calculated correspond to a thermal flow model with adiabatic journal and bearing surfaces.

Figures19 and 20 show the stiffness $(K_{\alpha\beta})_{\alpha,\beta=X,Y}$ and damping $(C_{\alpha\beta})_{\alpha,\beta=X,Y}$

coefficients versus increasing values of the angle of injection. The subindex (o) on the stiffness coefficients denotes values at zero frequency (ω=0), while the others are evaluated at a synchronous frequency, i.e. they contain the inertia coefficients and could be thought as dynamic stiffnesses equal to $K_{\alpha\beta o}-\omega^2 M_{\alpha\beta}$. Note that direct stiffness and damping coefficients vary little with the angle of fluid injection. On the other hand, the cross-coupled coefficients decrease steadily as the orifice supply angle increases with minimum values for tangential injection. For injection angles greater than 25° the WFR is zero and then negative indicating a bearing with unlimited stability for forward whirl motions.

CONCLUSIONS

The growth of an "all-fluid-film-bearing" technology for support of advanced cryogenic turbopumps demands the development of models and design tools, the testing of components, and the implementation of the technology on actual hardware. Conventional hybrid fluid film bearings have demonstrated adequate load support, direct stiffness and damping, but suffer from limited hydrodynamic stability which deters their use for high speed applications and flexible rotating structural systems. On the other hand, experiments on hybrid bearings with angled orifice injection have shown virtual elimination of cross-coupled stiffness coefficients and null or negative whirl frequency ratios (Franchek, 1992). No firm analysis was available at the time of the measurements, and hence, further technological developments since then were prevented.

The computational bulk-flow analysis for prediction of the performance and force coefficients of hybrid (combined hydrostatic - hydrodynamic) bearings

with angled orifice injection is the subject of the present research. The motion of a fluid through the thin film lands is governed by mass, momentum and energy transport equations for the flow velocities, pressure and temperature, along with state equations for the cryogen material properties. A simple model for the angled injection - orifice flow reveals that the fluid momentum exchange at the orifice discharge produces a pressure rise in the recess which retards the shear flow induced by journal rotation, and consequently, reduces cross - coupling forces. Zeroth-order and first-order diferential equations describe the fluid flow for a journal static position and dynamic perturbations, respectively Solution to the zeroth-order equations provides the bearing flow rate, shear torque and load capacity. Solutions to the first-order equations determine the linearized rotordynamic force coefficients at a specified whirl frequency.

The predictions from the model are compared with experimental measurements for two hybrid bearings with radial and 45° angled orifice injection. The test bearing nominal clearance is 125 μm and operates with water at 10.2 krpm to 24.6 krpm and with supply pressures from 4 to 7 MPa. Comparison of experiments and model calculations for load, flow rate and recess pressures are good and verify the soundness of the bulk-flow model. Correlations of model and test direct stiffness and damping coefficients are also favorable. The predictions show the same trends as the test values for the whirl frequency ratio and cross-coupled stiffness coefficients but large differences are apparent. Inertia force coefficients do not agree with the identified experimental values perhaps due to the large uncertainty in the measured coefficients. The experiments as well as the measurements demonstrate that the advantages of angled injection in hybrid bearings are lost as the journal speed increases and brings dominance of hydrodynamic over hydrostatic effects.

An application example for a liquid oxygen 6-recess hybrid bearing also verifies that a tangential angled orifice injection produces the lowest (negative) whirl frequency ratio and induces the largest cross-coupled stiffnesses which retard the development of forward whirl journal motions.

ACKNOWLEDGEMENTS
The support of NASA Lewis Research Center under NASA Grant NAG-1434 is gratefully acknowledged. Thanks to Mr. James Walker of NASA LeRC for his interest and patience. Professor Dara Childs is also acknowledged for his many contributions to this work.

REFERENCES:

Braun, M.J., Choy, F.K., and Y.M., Zhou, 1993, "The Effects of a Hydrostatic Pocket Aspect Ratio, Supply Orifice Position and Attack Angle on Steady-State Flow Patterns, Pressure and Shear Characteristics," ASME Journal of Tribology, Vol. 115, pp. 678-685.

Braun, M.J., M. Dzodzo, 1995, "Effects of the Feedline and the Hydrostatic Pocket Depth on the Flow Patterns and Pressure Distribution," ASME Journal of Tribology, Vol. 117, pp. 224-233.

Brown, R.D., J. A. Hart, 1986, "A Novel Form of Damper for Turbomachinery," Proceedings of the Workshop on Rotordynamic Instability Problems in High Performance Turbomachinery, Texas A&M University, pp. 325,348, NASA CP 2443.

Childs, D., and K. Hale, 1994, "A Test Apparatus and Facility to Identify the Rotordynamic Coefficients of High Speed Hydrostatic Bearings", ASME Journal of Tribology, Vol. 116, pp. 337-344.

Franchek, N., 1992, "Theory Versus Experimental Results and Comparisons for Five Recessed, Orifice Compensated, Hybrid Bearing Configurations," Texas A&M University, M.S. Thesis, TAMU Turbomachinery Laboratories, August 1992.

Franchek, N., and D. Childs, 1994, "Experimental Test Results for Four High Speed, High-Pressure, Orifice-Compensated Hybrid Bearings," ASME Journal of Tribology, Vol. 116, 2, pp. 285-290.

Franchek, N., D. Childs, and L. San Andres, 1995, "Theoretical and Experimental Comparisons for Rotordynamic Coefficients of a High-Speed, High-Pressure, Orifice-Compensated Hybrid Bearings," ASME Journal of Tribology, Vol. 117, 2, pp. 285-290.

Genge, G.G., Saville, M., and A. Gu, 1993, "Foil Bearing Performance in Liquid Nitrogen and Liquid Oxygen," AIAA/SAE/ASME/ASEE 29th Joint propulsion Conference and Exhibit, Monterrey, CA, June, Paper AIAA-93-2537.

Hill., D., E. Baskharone, and L. San Andres, 1995, "Inertia Effects in a Hybrid Bearing with a 45 degree Entrance Region," ASME Journal of Tribology, Vol. 117, 3, pp. 498-505.

Hirs, G. G., 1973, "A Bulk-Flow Theory for Turbulence in Lubricating Films," ASME Journal of Lubrication Technology, Vol.95, pp.135-146.

Kleynhans, G, and D. Childs, 1995, "The Acoustic Influence of Cell Depth on the Rotordynamic Characteristics of Smooth-Rotor/Honeycomb-Stator Annular Gas Seals," Seals Code Development Workshop, NASA Lewis Research Center, Cleveland, OH, June 15, 1995.

Kurtin, K., Childs, D., San Andres, L. and Hale, K., 1993, "Experimental versus Theoretical Characteristics of a High Speed Hybrid (combination

Hydrostatic and Hydrodynamic) Bearing," ASME Journal of Tribology, Vol. 115, 1, pp. 160-169.

Launder, B., and M. Leschziner, 1978, "Flow in Finite Width Thrust Bearings Including Inertial Effects," ASME Journal of Lubrication Technology, Vol. 100, pp. 330-345.

McCarty, R.D., 1986, NBS Standard Reference Data Base 12, Thermophysical Properties of Fluids, MIPROPS 86, Thermophysics Division, Center for Chemical Engineering, National Bureu of Standards, Colorado.

Mosher, P., and D. Childs, 1995, "Theory Versus Experiment for the Effect of Pressure Ratio on the Performance of an Orifice-Compensated Hybrid Bearing," 1995 ASME Design Engineering Technical Conference," DE-Vol 84-2, Vol.3-Part B., pp. 1119-1129.

Pelfrey, P., 1995, "Pratt & Whitney Fluid-Film Bearing and Seal Technology Development and Implementation," Seals Code Development Workshop, NASA Lewis Research Center, Cleveland, OH, June 15, 1995.

Redecliff, J.M. and J.H. Vohr, 1969, "Hydrostatic Bearings for Cryogenic Rocket Engine Pumps," ASME Journal of Lubrication Technology, pp. 557-575.

San Andres, L.A., 1990, "Turbulent Hybrid Bearings with Fluid Inertia Effects", ASME Journal of Tribology, Vol. 112, pp. 699-707

San Andres, L., 1992, "Analysis of Turbulent Hydrostatic Bearings with a Barotropic Fluid," ASME Journal of Tribology, Vol. 114, 4,pp. 755-765,1992.

San Andres, L., 1993, "Thermohydrodynamic Analysis of Cryogenic Liquid Turbulent Flow Film Bearings for Cryogenic Applications," Research Progress Report to NASA Lewis Research Center, NASA Grant NAG3-1434, December.

San Andres, L., 1995a, "Thermohydrodynamic Analysis of Fluid Film Bearings for Cryogenic Applications," AIAA Journal of Propulsion and Power, Vol. 11, 5, pp. 964-972.

San Andres, L., 1995b, "Two Pad Axially Grooved Hydrostatic Bearing," U.S. Patent 5,433,528, July, 18.

San Andres, L., 1995c, "Turbulent Flow, Flexure-Pivot Hybrid Bearings for Cryogenic Applications," 1995, STLE/ASME Tribology Conference, Orlando, ASME Journal of Tribology, ASME Paper 95-TRIB-14.

San Andres, L., 1995d, "Turbulent Flow Foil Bearings for Cryogenic Applications," ASME Journal of Tribology, Vol. 117, 1, pp. 185-195.

Tondl, A., 1967, "Bearings with a Tangential Gas Supply," Gas Bearing Symposium, University of Southampton, Dept. of Mechanical Engineering.

Van Doormaal, J.P., and D. Raithby, 1984, "Enhancements of the SIMPLE Method

for Predicting Incompressible Fluid Flows," Numerical Heat Transfer, Vol. 7, pp. 147-163.

Yang, Z., L. San Andres and D. Childs, 1995, "Thermohydrodynamic Analysis of Process Liquid Hydrostatic Bearings in Turbulent Regime, Part I: The Model and Perturbation Analysis, Part II: Numerical Solution and Results," ASME Journal of Applied Mechanics, Vol. 62, 3, pp. 674-684.

Table 1. Description of water lubricated orifice compensated hybrid bearing tested by Franchek and Childs (1994).

No of recesses (Nrec) 5
Clearance nominal (C) 125.4 μm (0.005 in)
Diameter (D) 76.2 mm (3 in)
Length (L) 76.2 mm (3 in)
Land roughness (peak-peak) 0.33 μm (13 μin)

Recess dimensions: square (l) 27 mm x (b) 27 mm x 254 μm (depth)
Supply volume Vs = 0.1289 dm^3

Orifice at midplane of recess.
diameter d=2.49 mm, C_d=varies (see below)
Radial and angled injection (45°)

Lubricant: water at Ts=328.3 °K
Viscosity (μ) 0.4929E-3 Pa.s
Density (ρ) 986.26 kg/m^3
Discharge pressure Pa: 0.0 MPa (0 psig)

Empirical parameters:
Entrance loss factors ξ_x, ξ_y= 0.0, Inlet swirl α=0.5

Test Conditions and estimated parameters at centered operation

Angled injection:

Speed Kcpm	P_s MPa	C μm	Q lt/min	Pr_{ave} MPa	C_d	Re_c ($\rho\Omega Rc/\mu$)	Re_a ($Q/\pi D\mu$)
10.2	4.133	122.8	79.94	1.128	0.700	9,998.0	11,136.0
	5.519	124.4	92.21	1.252	0.680	10,129.1	12,845.6
.	6.877	124.9	102.29	1.434	0.660	10.169.8	14,249.8
17.4	4.154	120.5	79.60	1.866	0.800	16,737.3	11,088.3
	5.521	121.5	91.67	2.148	0.763	16,876.2	11,088.9
.	6.846	122.7	101.75	2.316	0.726	17,042.0	14,174.0
24.6	4.135	119.4	78.07	2.424	0.907	23,447.2	10.875.8
	5.532	120.8	92.21	2.870	0.859	23,722.0	12,942.4
.	6.844	117.1	101.38	3.206	0.808	23,000.0	14,123.0

Radial injection:

Speed Kcpm	P_s MPa	C μm	Q lt/min	PR_{ave} MPa	C_d	Re_c ($\rho\Omega Rc/\mu$)	Re_a ($\rho Q/\pi D\mu$)
10.2	4.120	119.6	84.89	1.759	0.840	9,738.2	11,825.0
	5.519	119.4	98.70	2.163	0.820	9,722.0	13,749.0
.	6.889	118.2	110.86	2.342	0.790	9,624.3	15,443.0
17.4	4.118	116.5	82.37	2.199	0.904	16,181.7	11,474.1
	5.494	116.5	97.91	2.675	0.887	16,181.7	13,639.0
.	6.889	115.7	109.84	3.100	0.856	16,070.6	15,300.7
24.6	4.141	111.9	73.11	2.550	0.881	21,974.3	10,184.2
	5.494	115.8	91.64	3.164	0.912	22,740.2	12,765.5
.	6.904	114.2	105.88	3.693	0.900	22,426.0	14,749.1

(*) Cd values estimated from measured flow rate and average recess pressures

Table 2. Description of 6 pad/recess liquid oxygen hybrid bearing with angled injection

No of recesses (Nrec)	6
Clearance nominal (C)	76.2 μm (0.003 in)
Diameter (D)	92.7 mm (3.65 in)
Pad arc length	40.45 mm (1.59 in) [50°]
Length (L)	37.1 mm (1.46 in)
Land roughness (peak-peak)	smooth

Recess dimensions: square (l) 19 mm x (b) 19 mm x 228 μm (depth)
Supply volume Vs = 0.0 dm^3

Orifice at midplane of recess.
diameter d=2.328 mm, C_d=1.0
Angle of injection (-10° to 90°)

Rotational speed: 25,000 rpm (2,618 rad/s)

Lubricant: liquid oxygen at Ts= 90 °K (supercritical conditions)
Supply pressure P_s=26.71 MPa (3,874 psi)
Exit pressure P_a= 8.81 MPa (1,278 psi)

	Supply	Exit	
Viscosity (μ)	0.2459E-3	0.2125E-3	Pa.s
Density (ρ)	1,192	1,160	kg/m^3

Empirical parameters:
Entrance loss factors ξ_x, ξ_y= 0.0, Inlet swirl α=0.5, C_d=1.0

Circumferential flow Reynolds number, $Re_c = \rho\Omega Rc/\mu$ = 44,822

Nominal axial flow Reynolds number, $Re_a = Q/\pi D\mu$ = 48,972

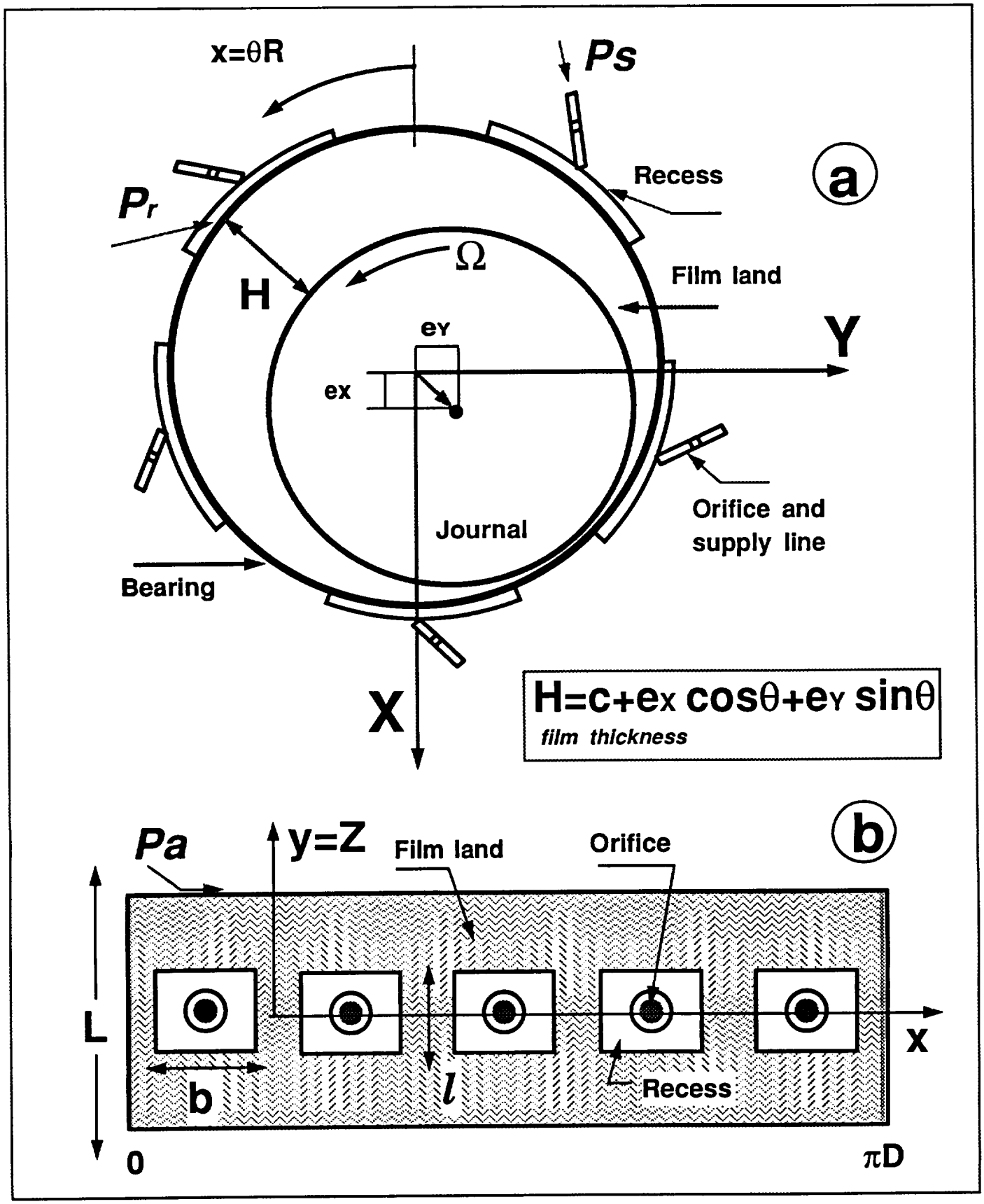

Figure 1. Geometry of an orifice compensated – angled injection hybrid bearing.
a) Axial View and Coordinate System, b) Unwrapped Bearing Surface

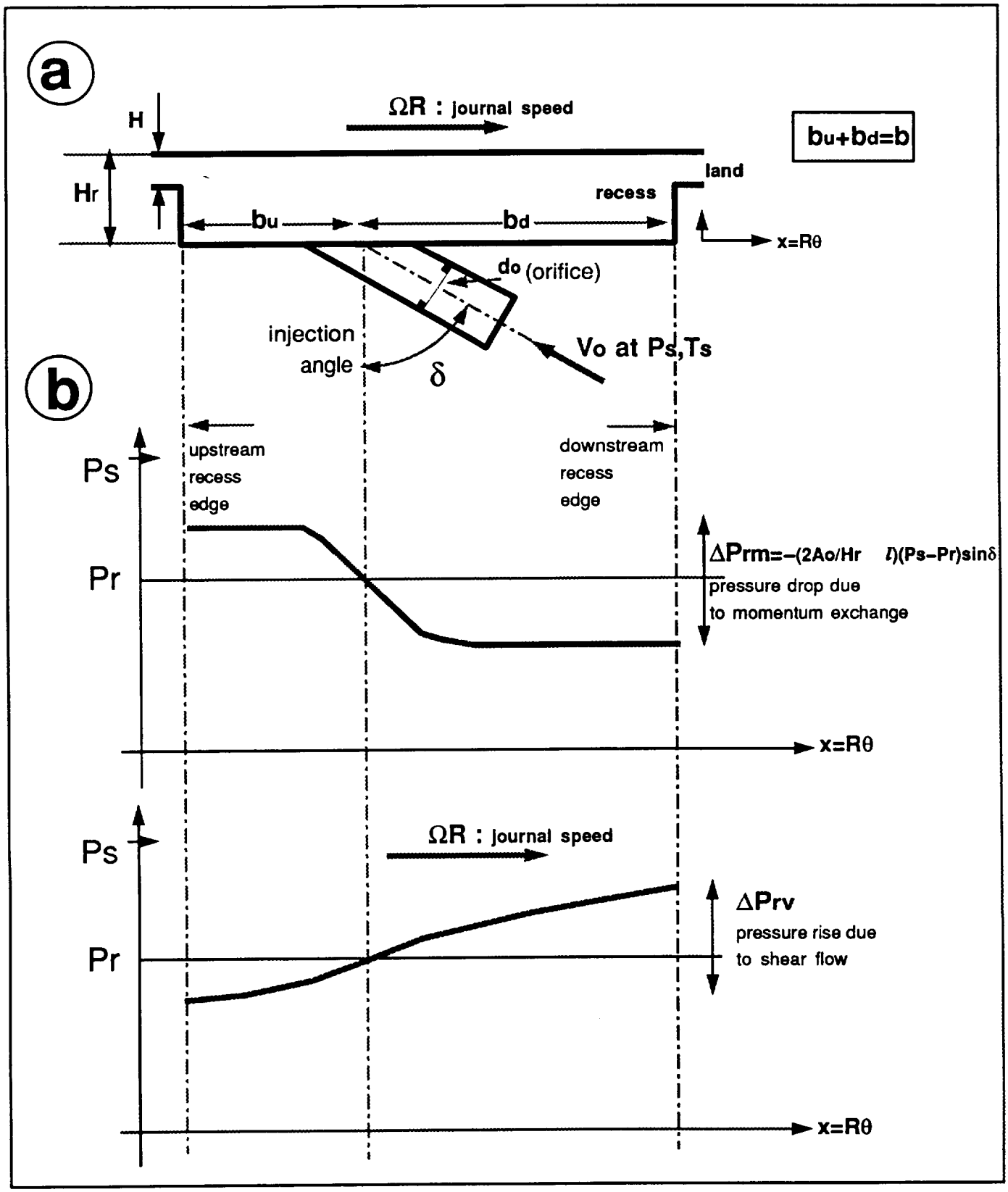

Figure 2. **(a) Description of hydrostatic recess with angled injection**
(b) Assumed pressure field within hydrostatic recess

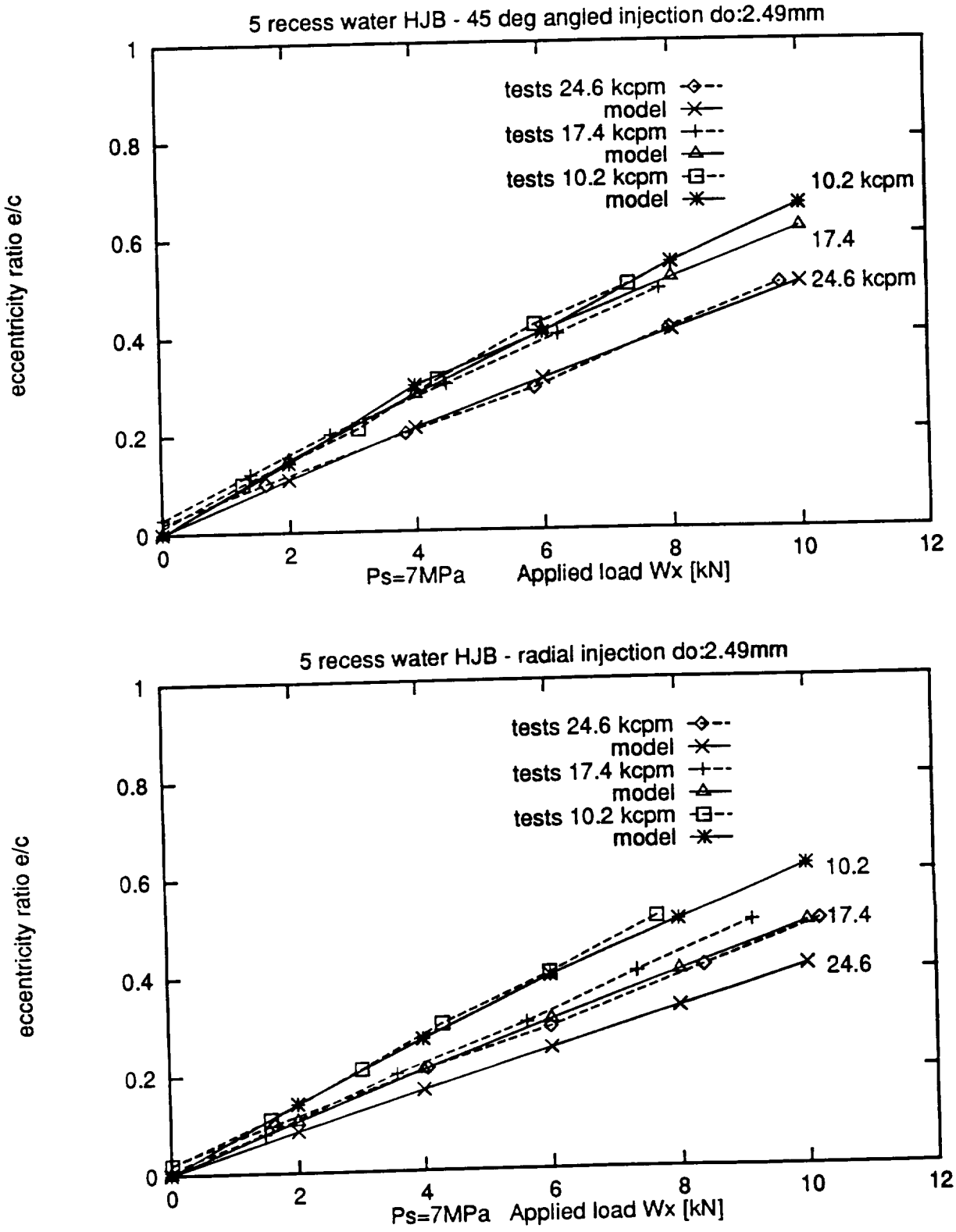

Figure 3. Journal eccentricity vs. applied load Wx for water - 5 recess hybrid bearing. Comparison to experimental results.
(a) top - 45 degree angled injection (b) bottom - radial injection

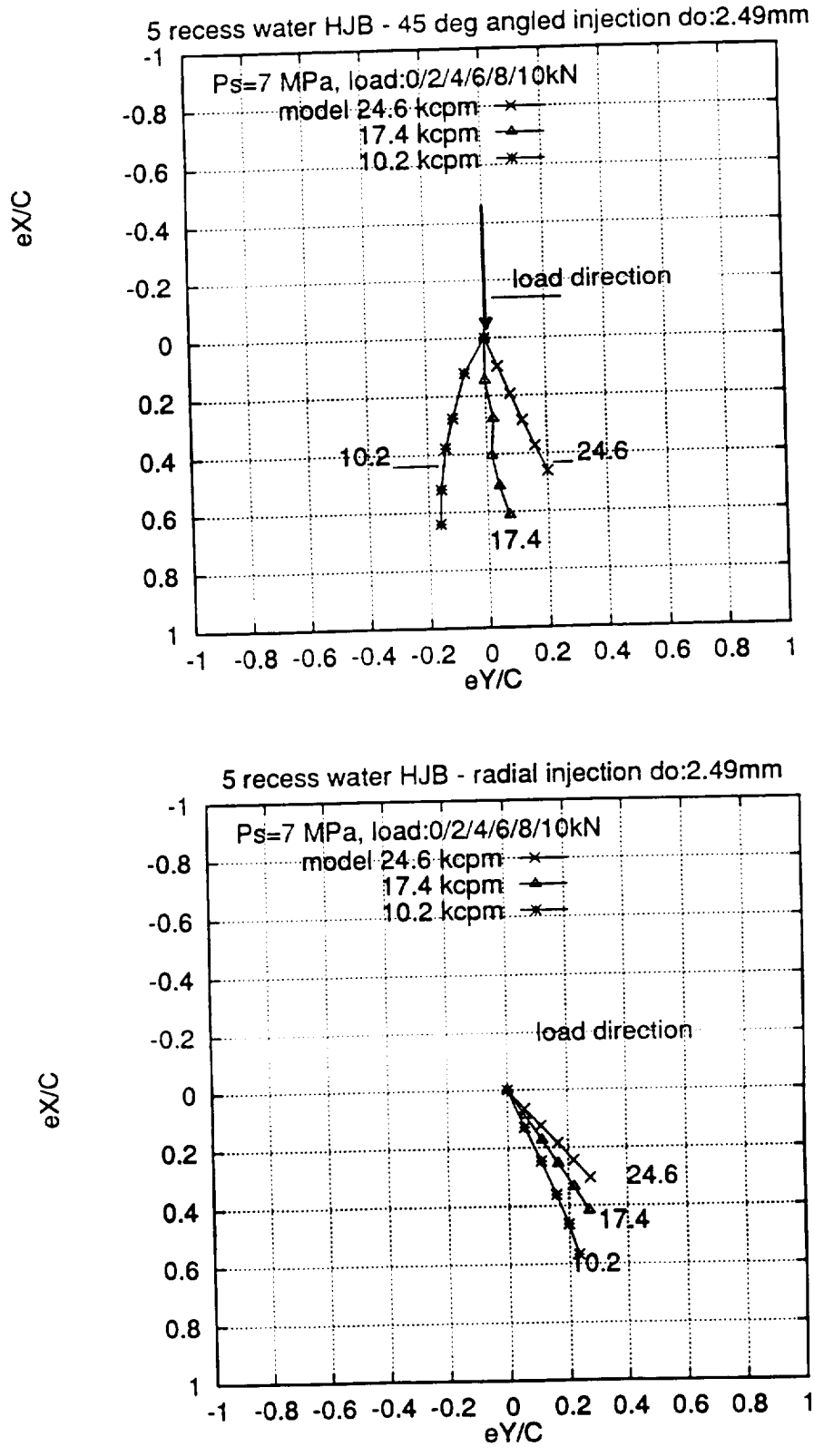

Figure 4. Journal center locus for water - 5 recess hybrid bearing. Numerical predictions for increasing loads.
(a) top - 45 degree angled injection (b) bottom - radial injection

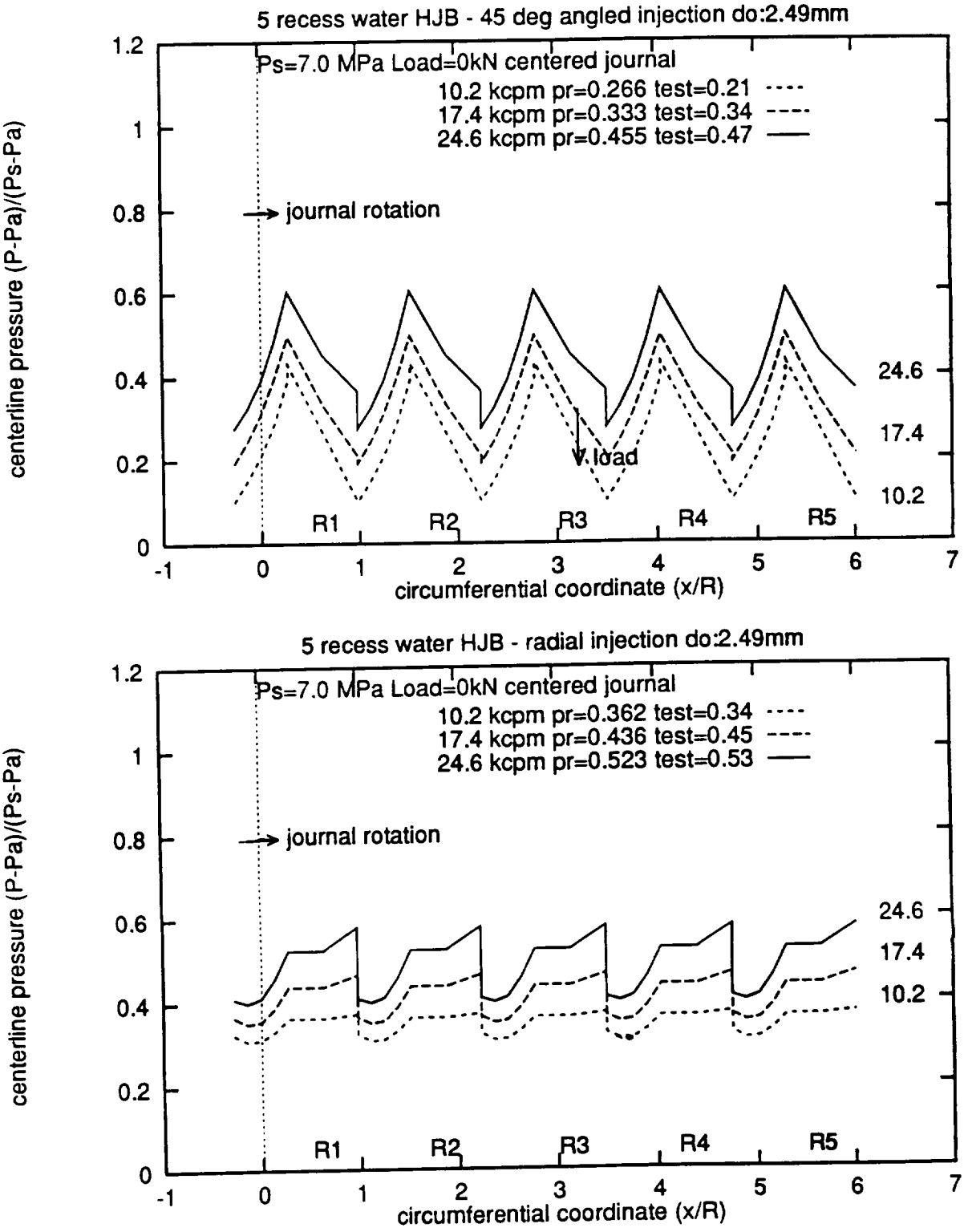

Figure 5. Numerical predictions for centerline pressure at zero load, Ps = 7 MPa, water - 5 recess hybrid bearing.
(a) top - 45 degree angled injection (b) bottom - radial injection

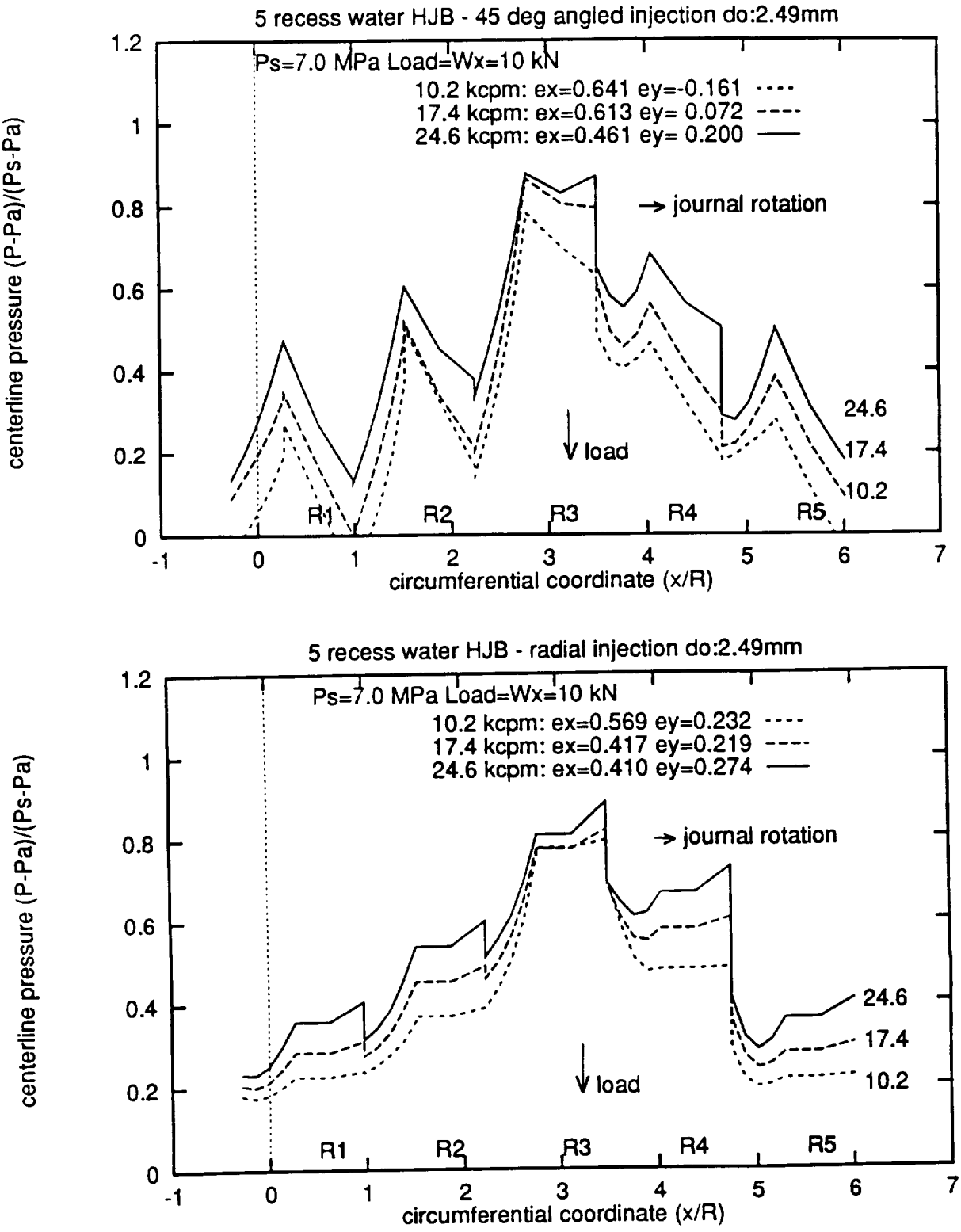

Figure 6. Numerical predictions for centerline pressure at 10 kN load, Ps = 7 MPa, water - 5 recess hybrid bearing.
(a) top - 45 degree angled injection (b) bottom - radial injection

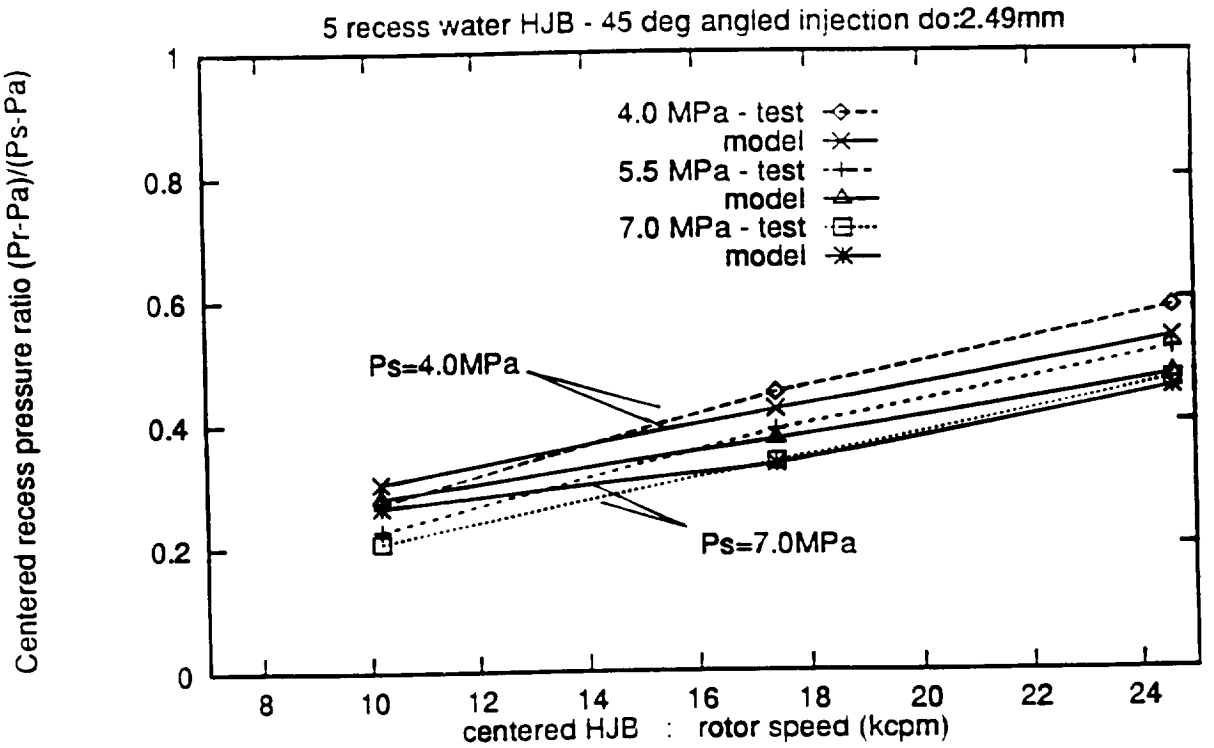

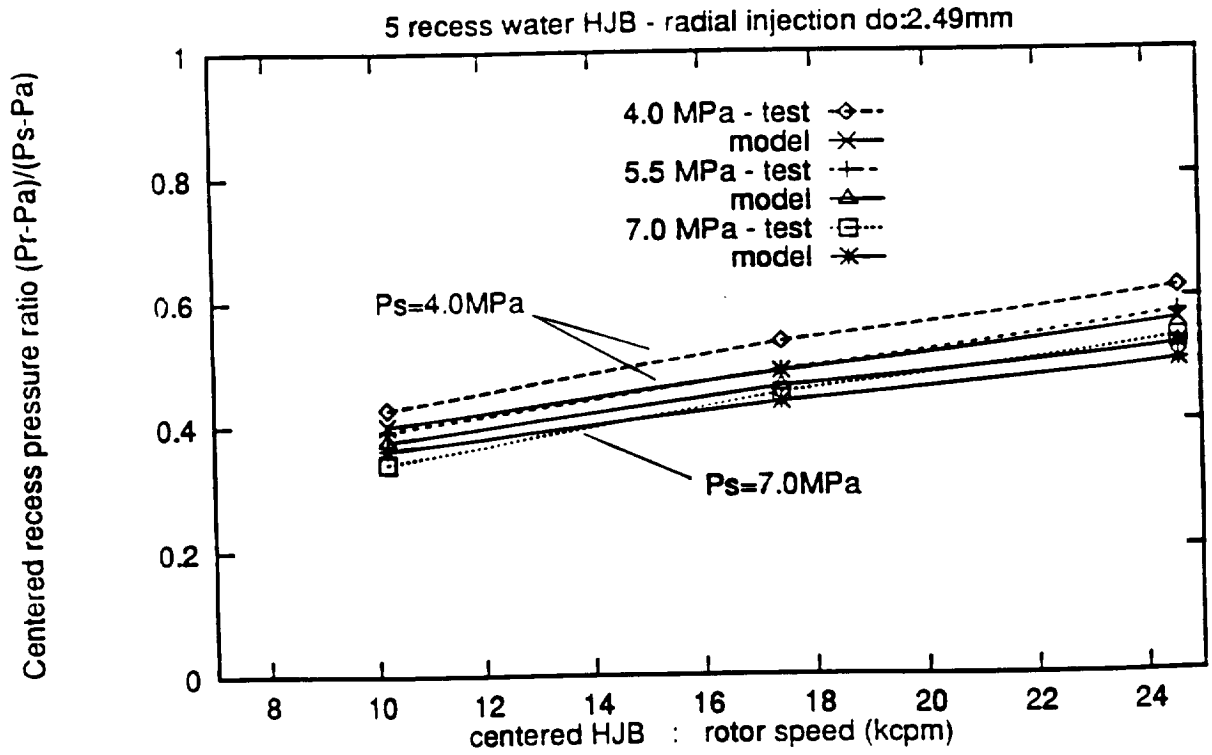

Figure 7. Centered recess pressure ratio (Pr-Ps)/(Ps-Pa) for water - 5 recess hybrid bearing. Comparison to experimental results.
(a) top - 45 degree angled injection (b) bottom - radial injection

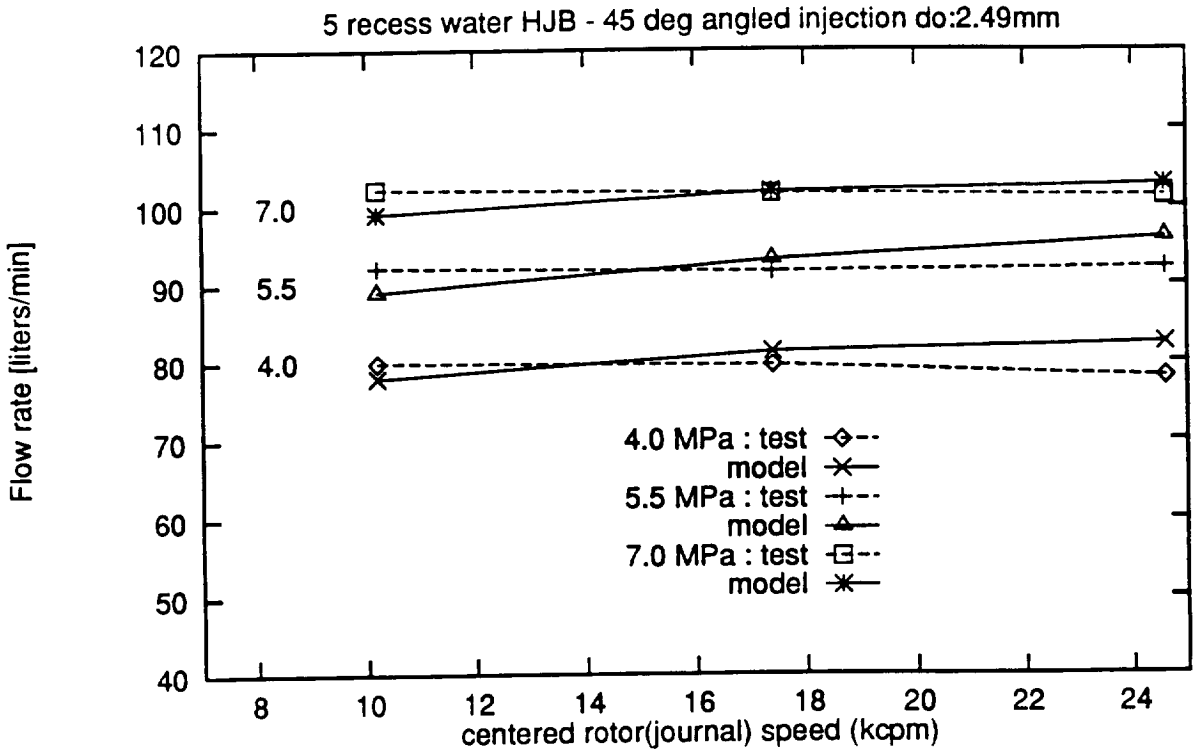

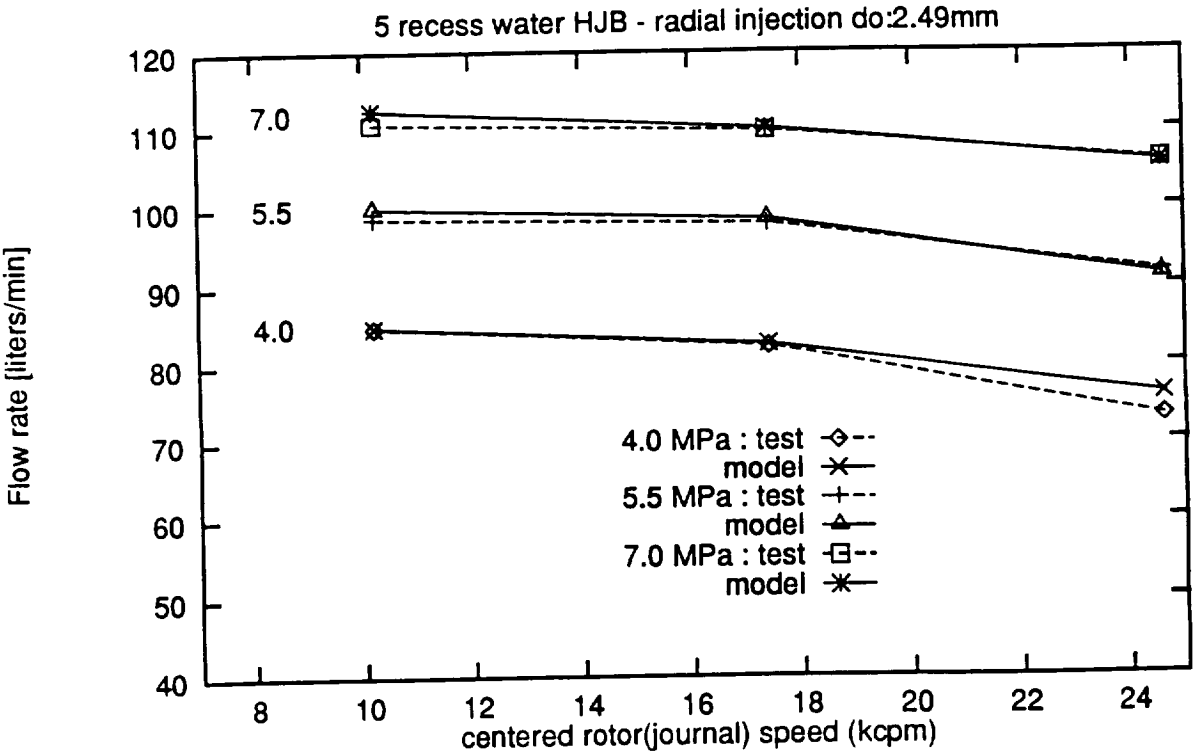

Figure 8. Bearing flow rate vs. journal speed for water - 5 recess hybrid bearing. Comparison to experimental results.
(a) top - 45 degree angled injection (b) bottom - radial injection

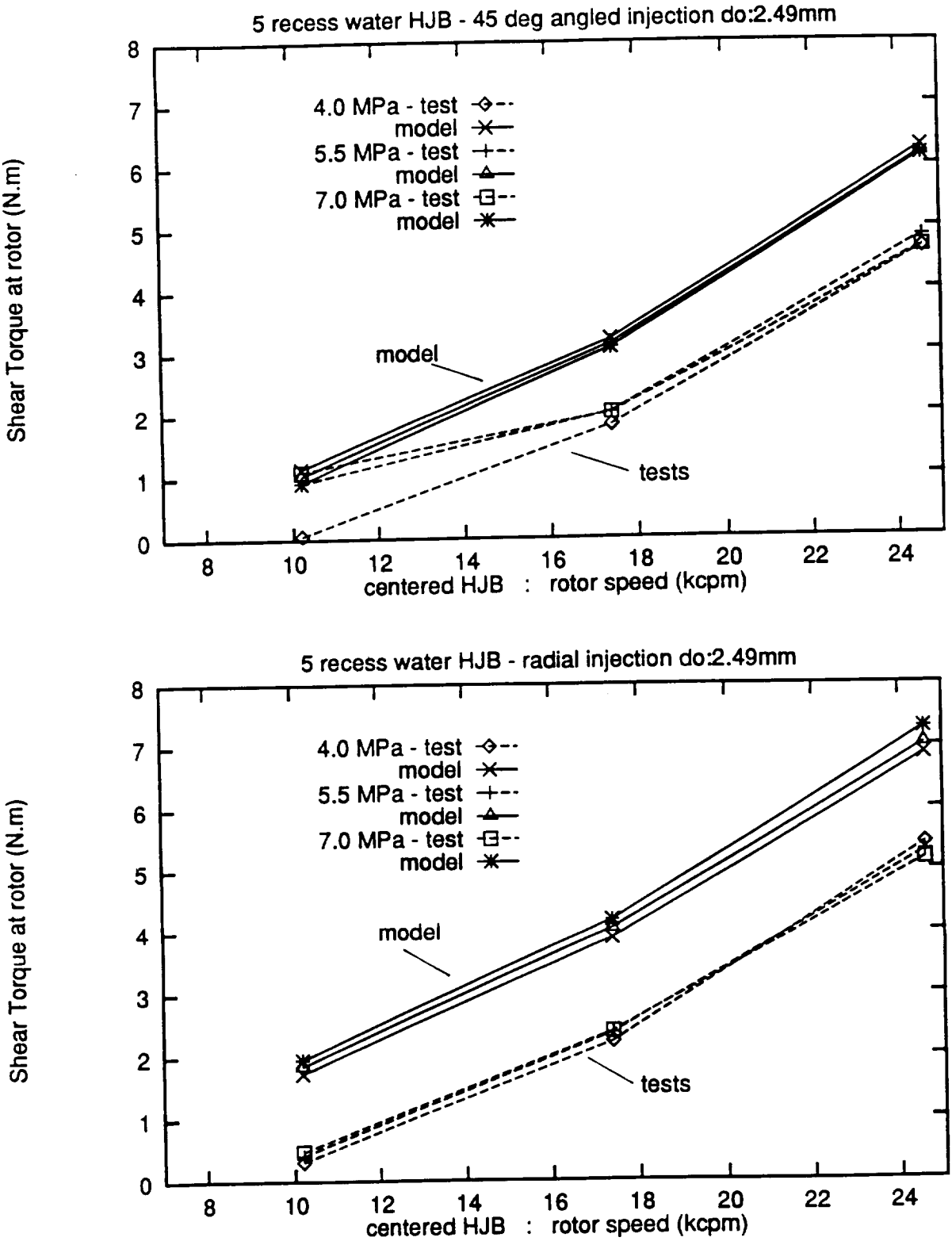

Figure 9. Shear torque at journal vs. speed for water - 5 recess hybrid bearing. Comparison to experimental results.
(a) top - 45 degree angled injection (b) bottom - radial injection

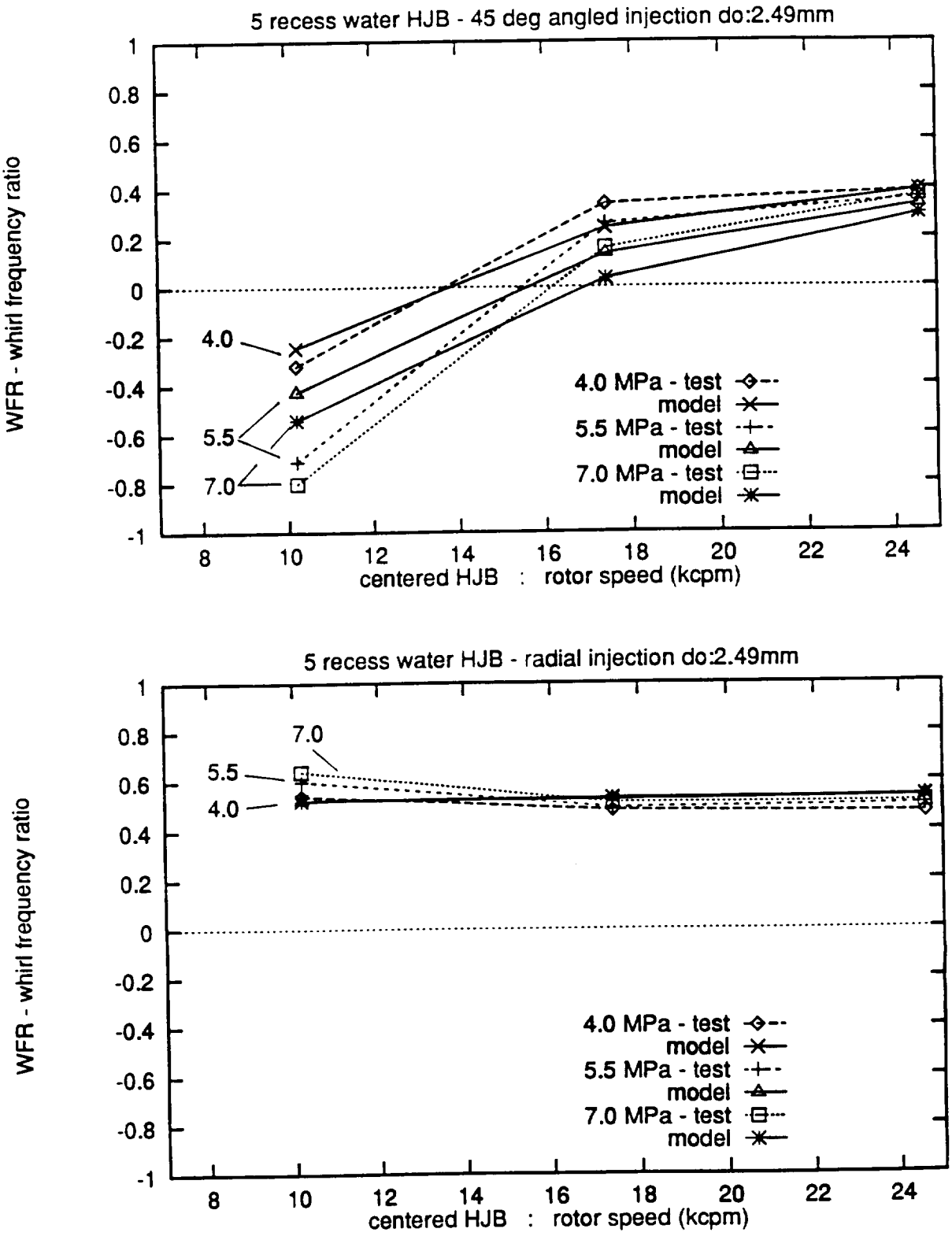

Figure 10. Whirl frequency ratio vs. journal speed for water - 5 recess hybrid bearing. Comparison to experimental results.
(a) top - 45 degree angled injection (b) bottom - radial injection

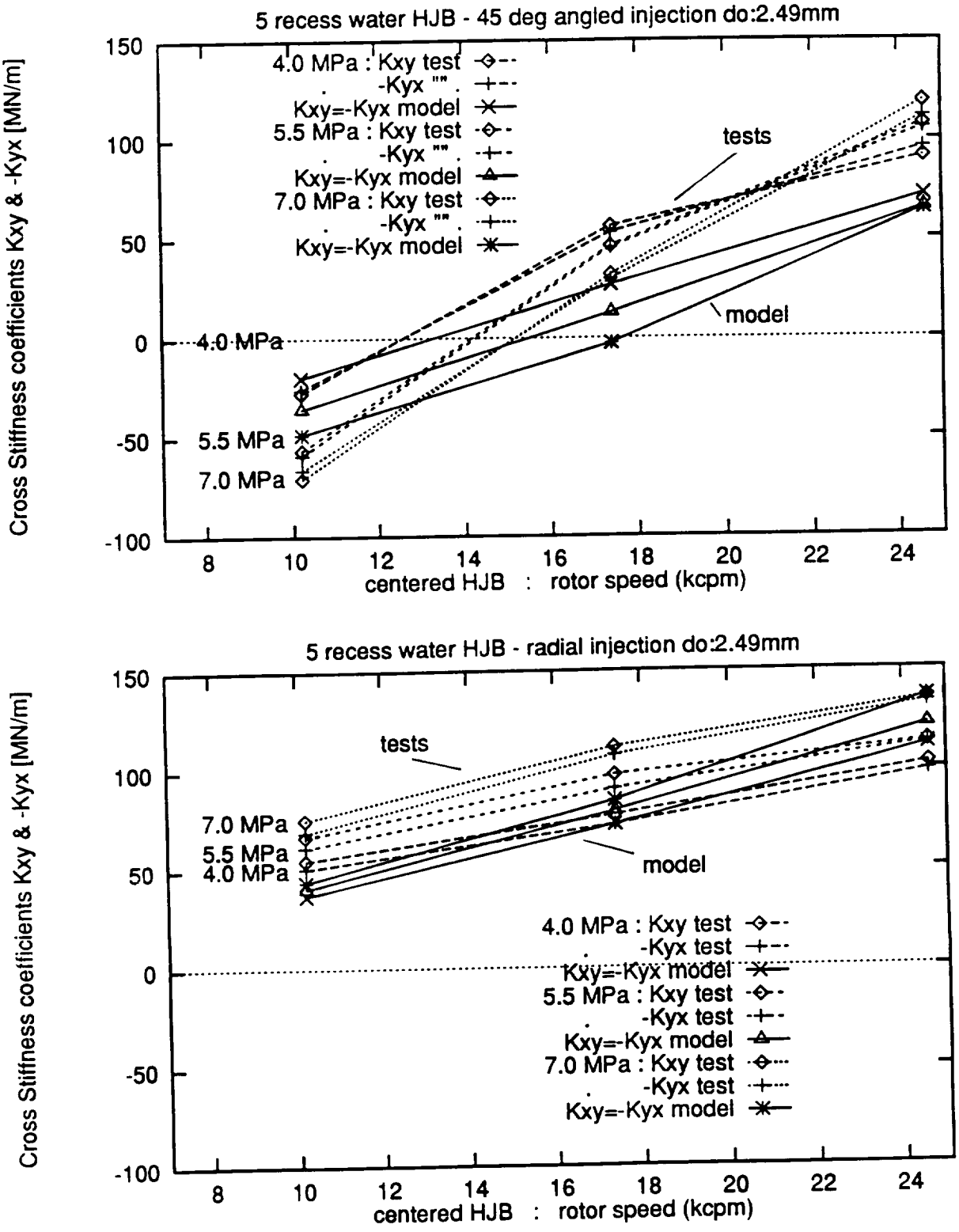

Figure 11. Cross-stiffness coefficients (KXY, -KYX) vs. journal speed for water - 5 recess hybrid bearing. Comparison to experimental results.
(a) top - 45 degree angled injection (b) bottom - radial injection

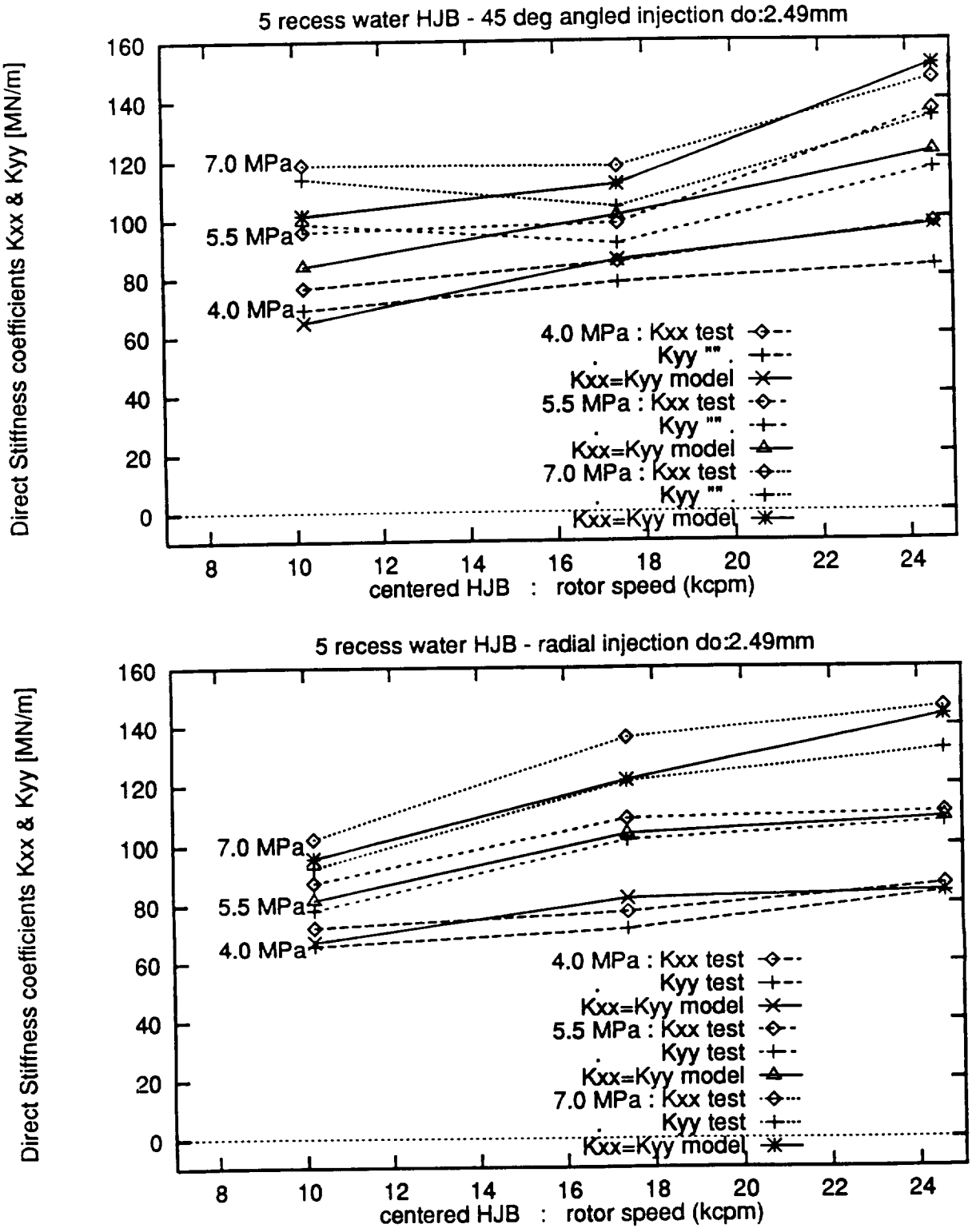

Figure 12. Direct stiffness coefficients (Kxx, Kyy) vs. journal speed for water - 5 recess hybrid bearing. Comparison to experimental results.

(a) top - 45 degree angled injection (b) bottom - radial injection

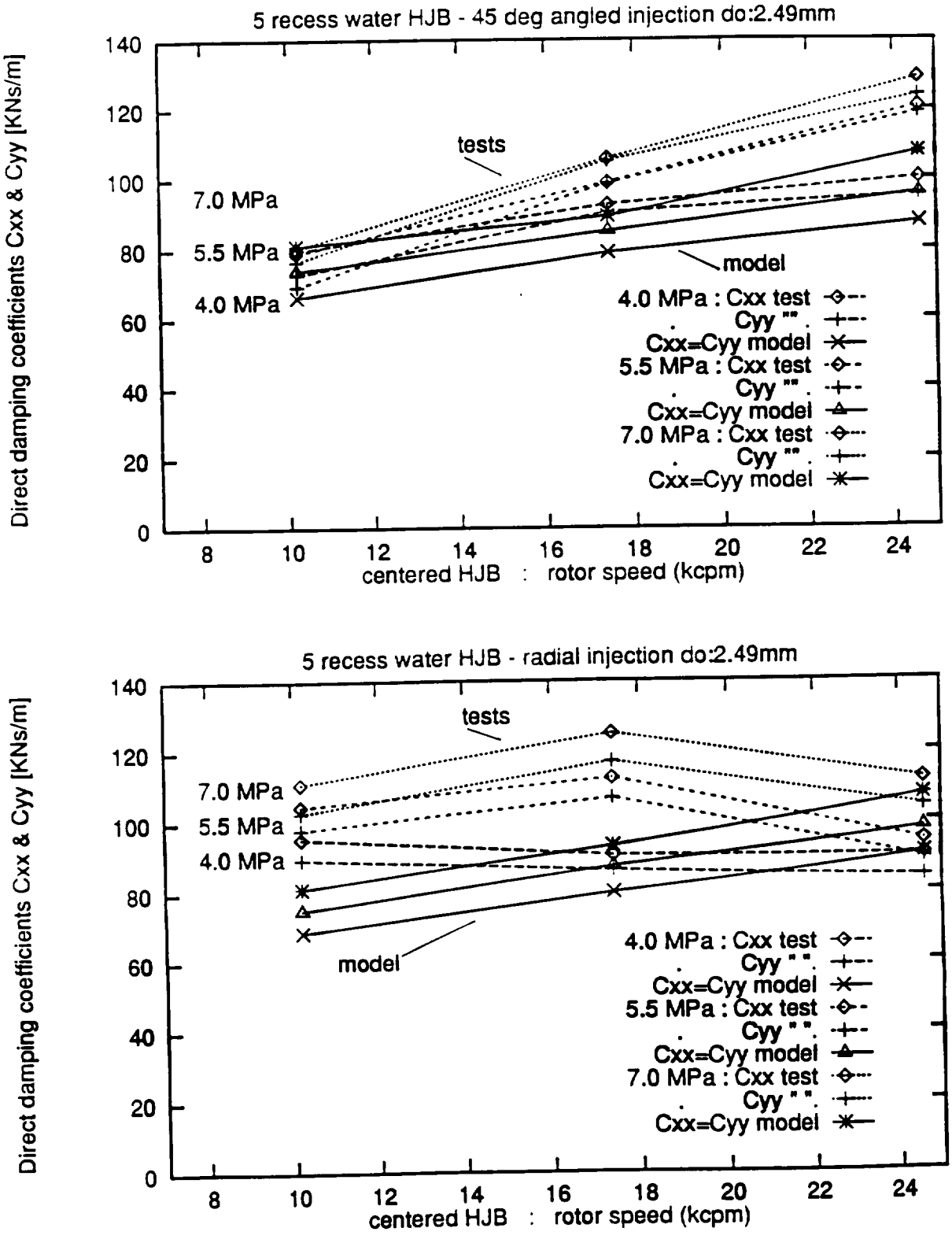

Figure 13. Direct damping coefficients (CXX, CYY) vs. journal speed for water - 5 recess hybrid bearing. Comparison to experimental results.

(a) top - 45 degree angled injection (b) bottom - radial injection

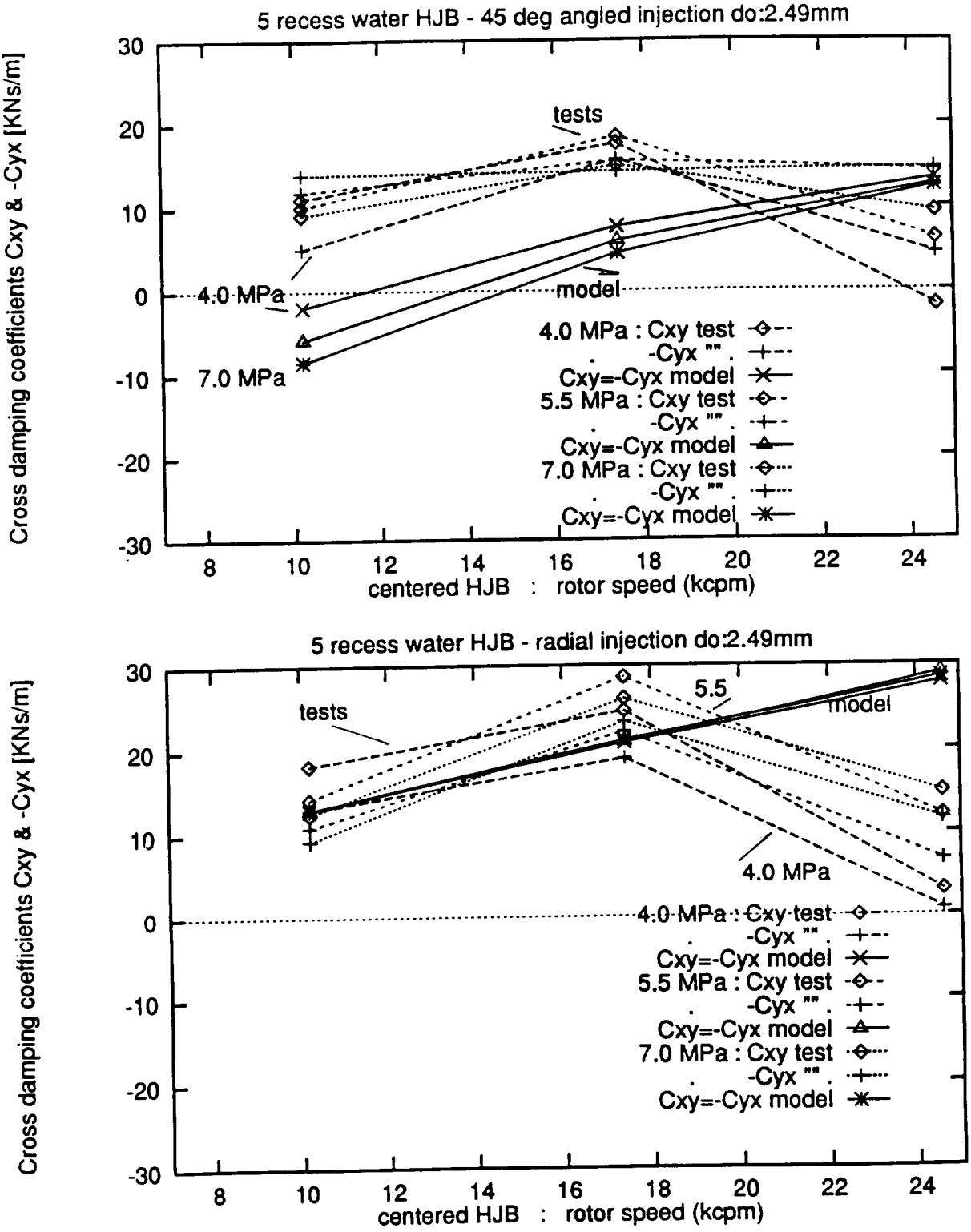

Figure 14. Cross-damping coefficients (Cxy, -Cyx) vs. journal speed for water - 5 recess hybrid bearing. Comparison to experimental results.

(a) top - 45 degree angled injection (b) bottom - radial injection

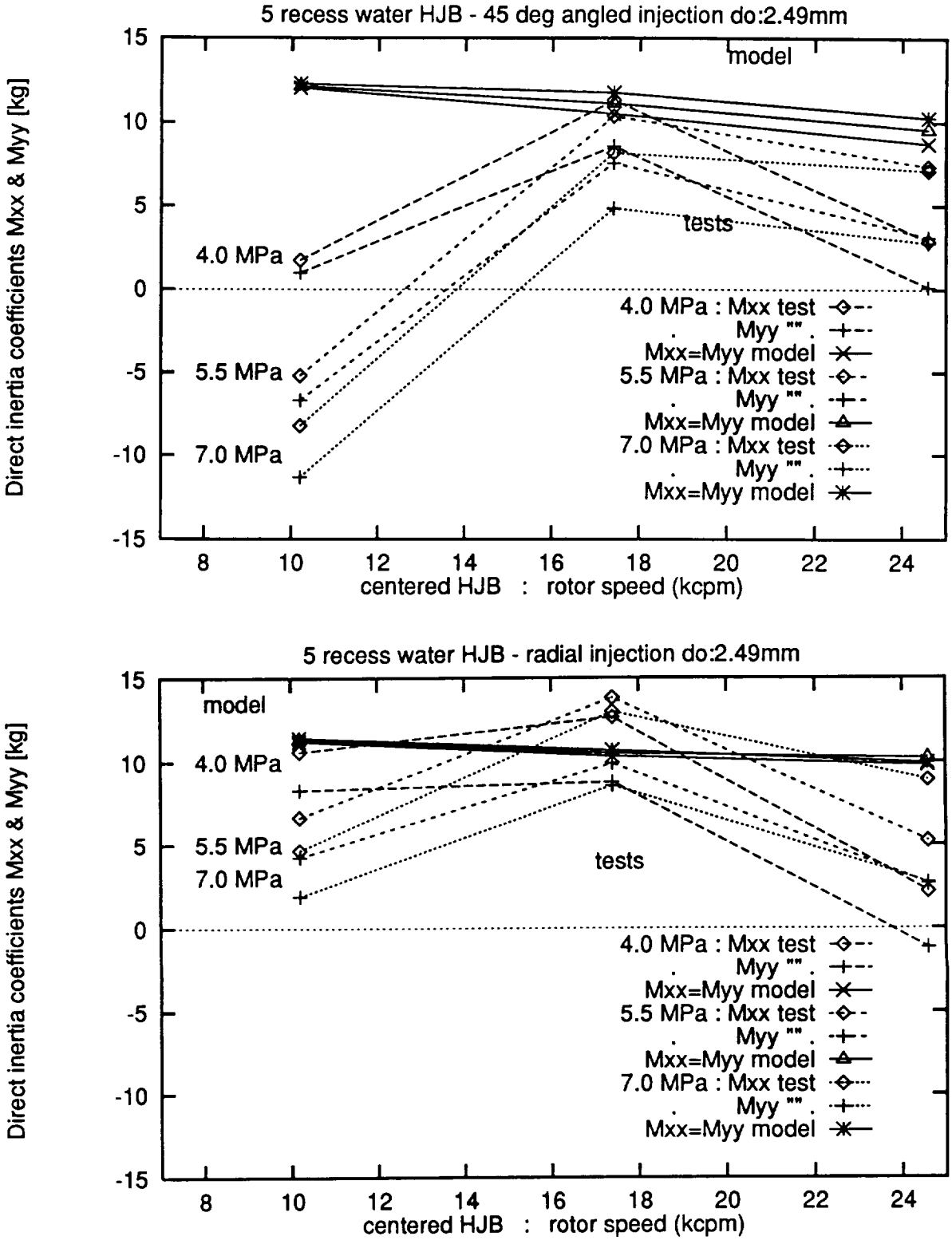

Figure 15. Direct inertia coefficients (MXX, MYY) vs. journal speed for water - 5 recess hybrid bearing. Comparison to experimental results.

(a) top - 45 degree angled injection (b) bottom - radial injection

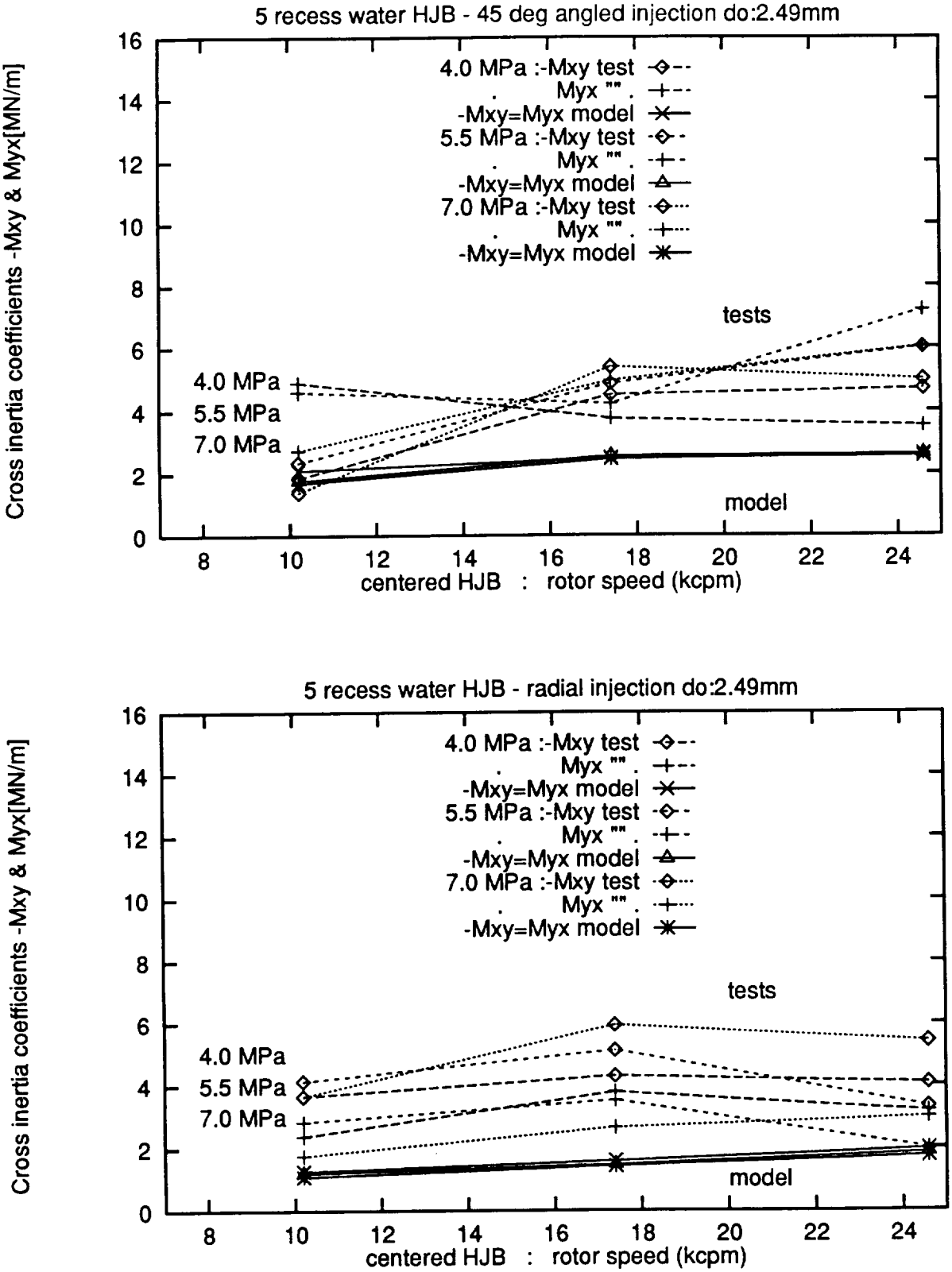

Figure 16. Cross-Inertia coefficients (MYX, -MXY) vs. journal speed for water - 5 recess hybrid bearing. Comparison to experimental results.

(a) top - 45 degree angled injection (b) bottom - radial injection

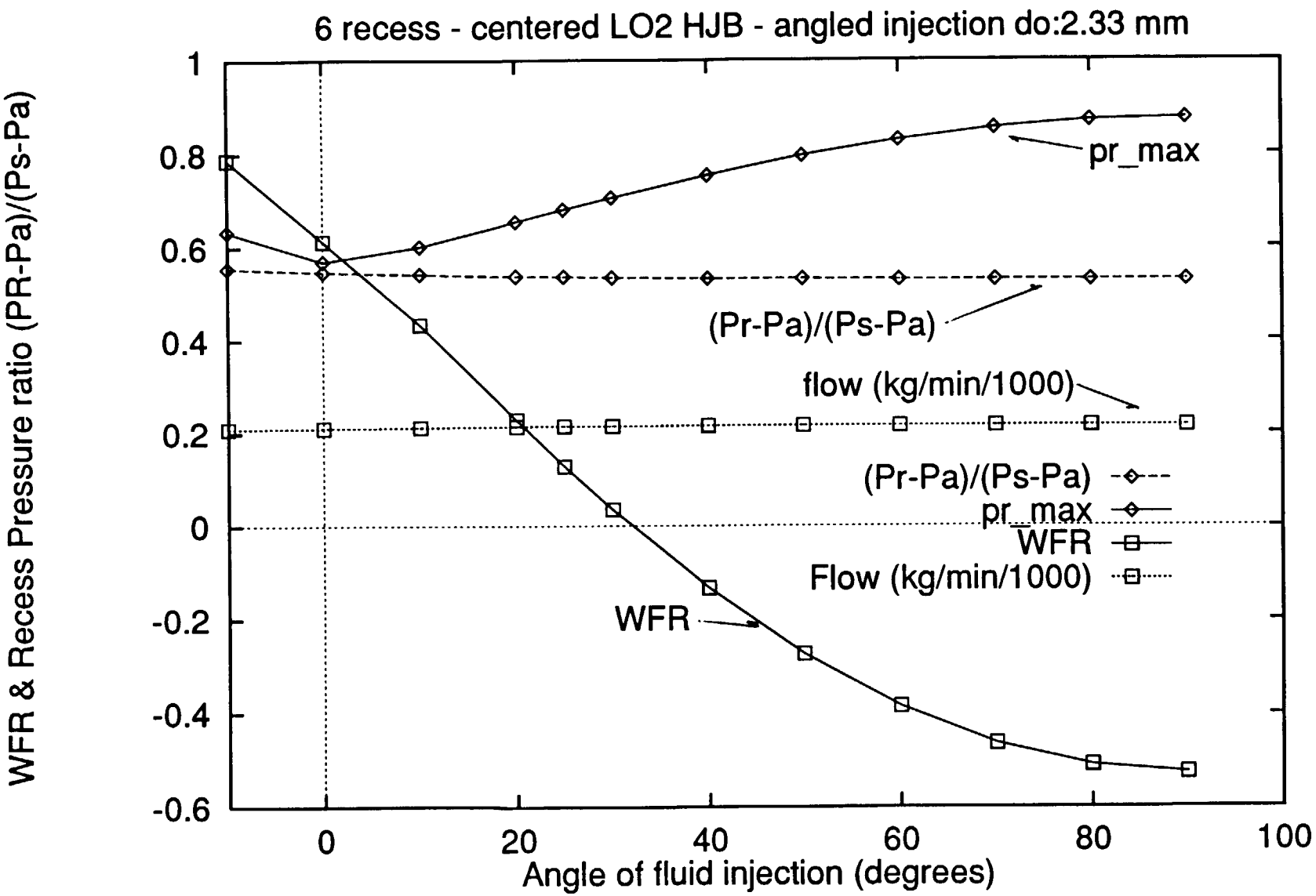

Figure 17. Flow rate, whirl frequency and recess pressure ratios vs. angle of fluid injection for 6 recess LO2 hybrid bearing (Ps-Pa=17.9 MPa, Ts=90 K, 25 krpm)

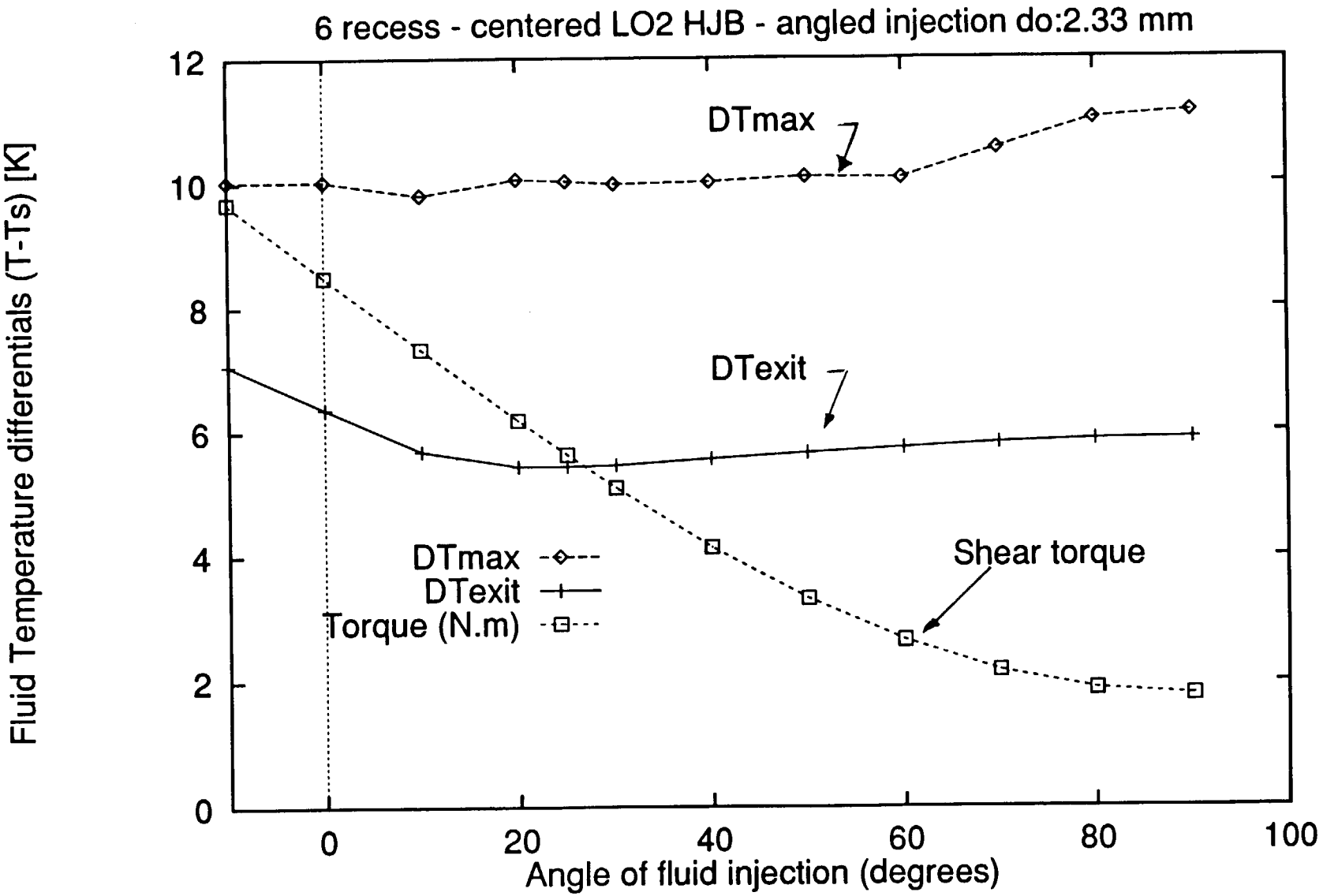

Figure 18. Shear torque, maximum and exit temperature differences vs. angle of fluid injection for 6 recess LO_2 hybrid bearing
(Ps-Pa=17.9 MPa, Ts=90 K, 25 krpm)

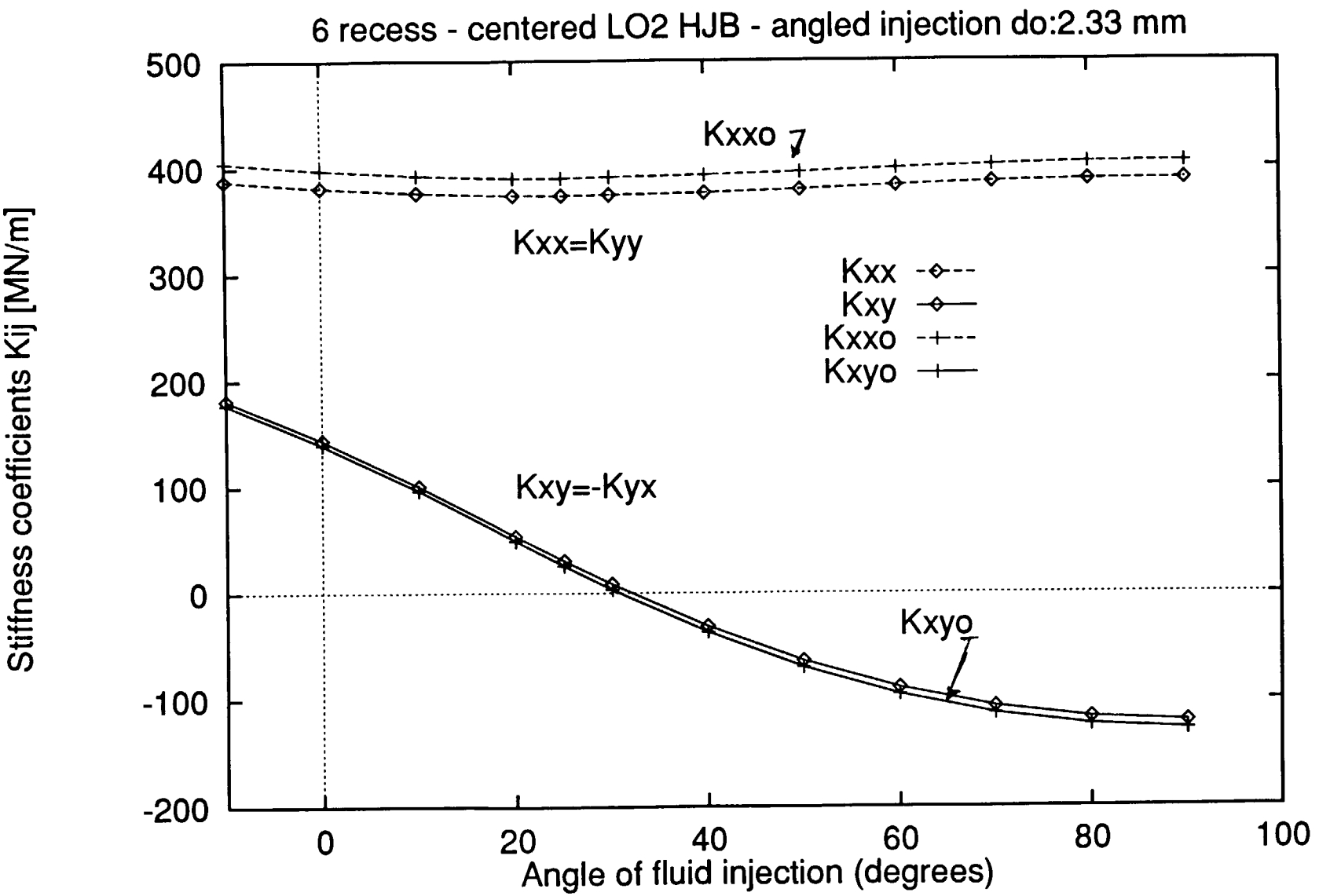

Figure 19. Stiffness coefficients (KXX=KYY), (KXY=-KYX) vs. angle of fluid injection for 6 recess LO2 hybrid bearing (Ps-Pa=17.9 MPa, Ts=90 K, 25 krpm)

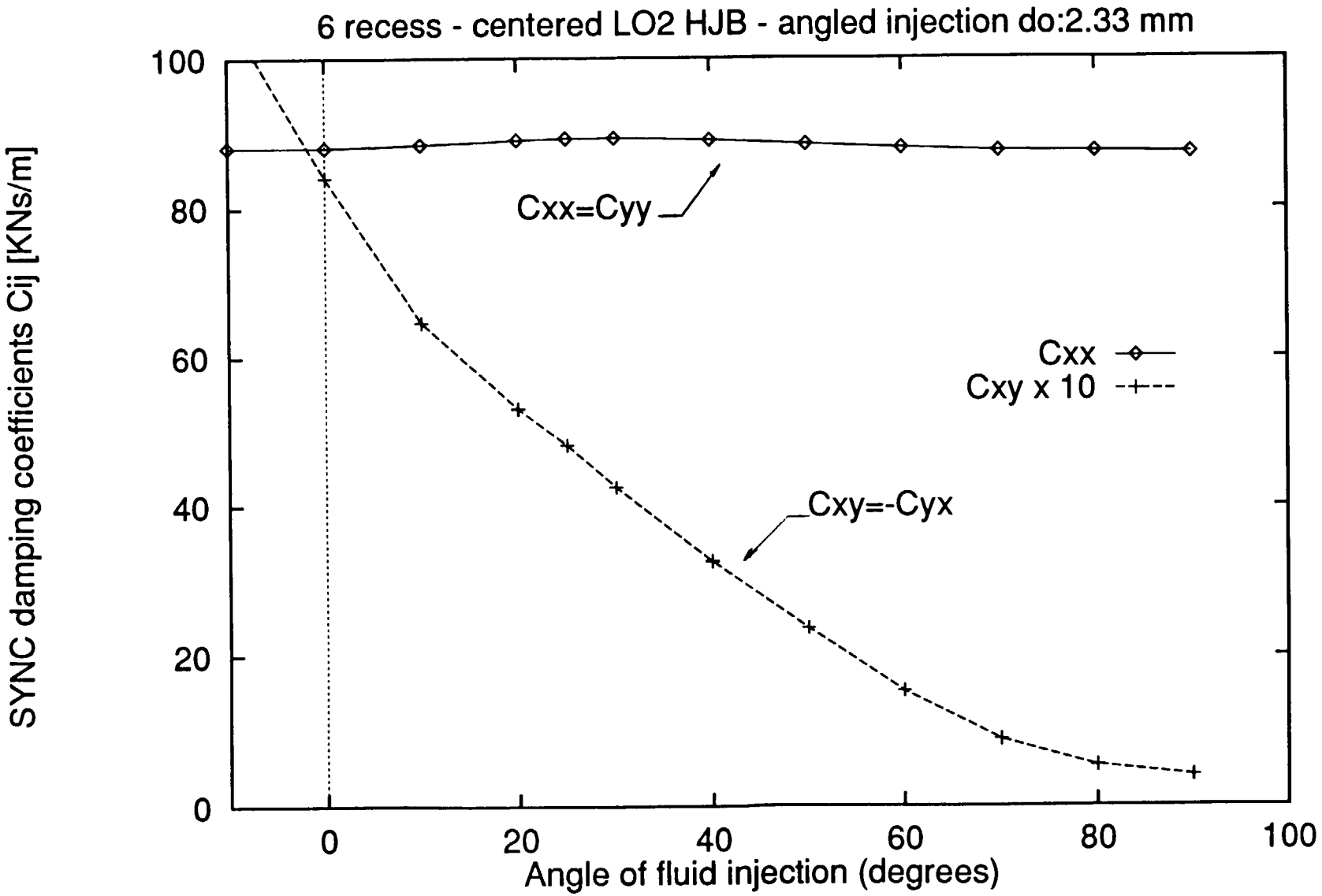

Figure 20. Damping coefficients (CXX=CYY), (CXY=-CYX) vs. angle of fluid injection for 6 recess LO2 hybrid bearing (Ps-Pa=17.9 MPa, Ts=90 K, 25 krpm)